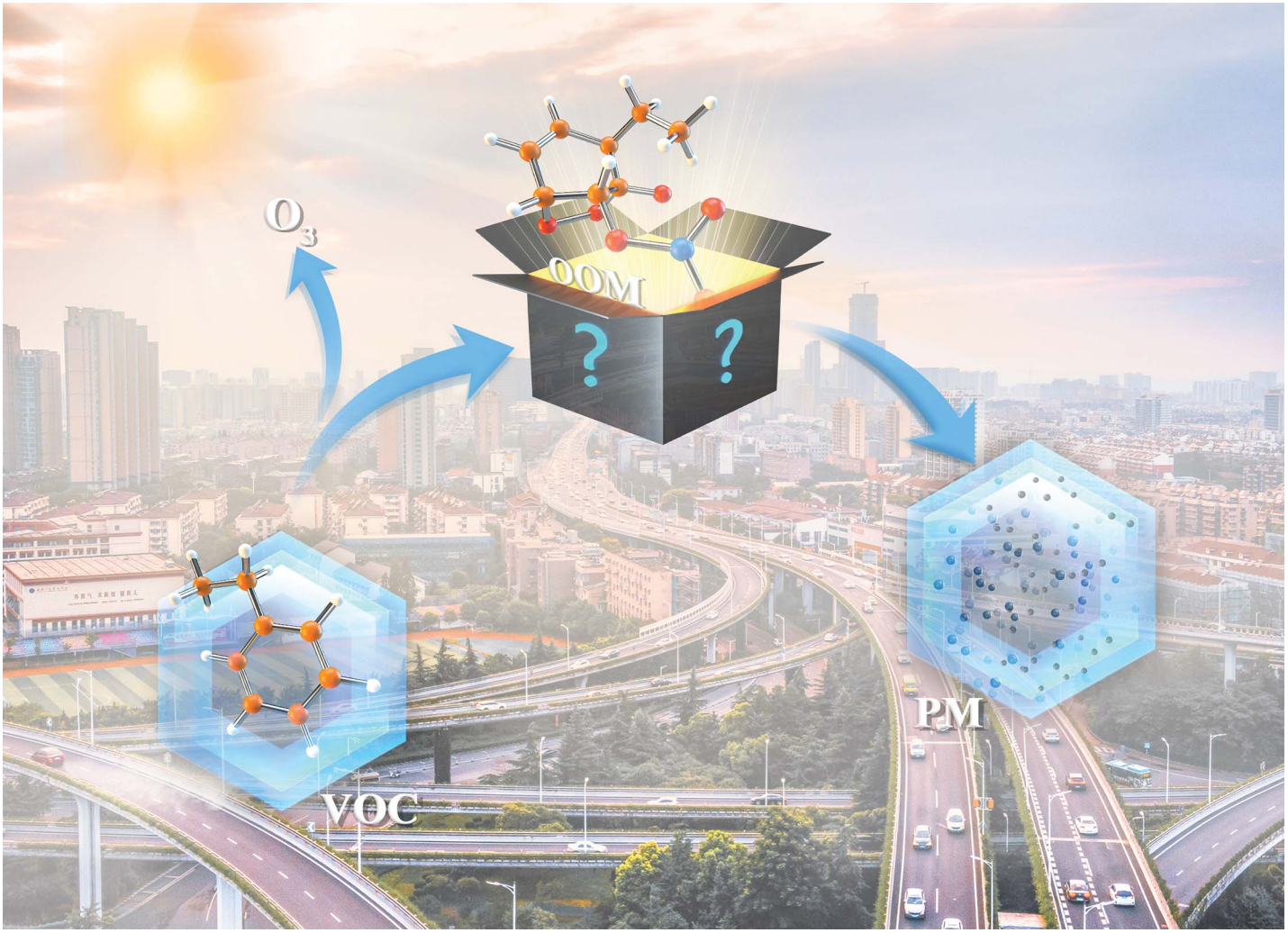


**Showcasing research from Professor Nie's laboratory, School of Atmospheric Sciences, Nanjing University, Nanjing, China.**

Exploring condensable organic vapors and their co-occurrence with $PM_{2.5}$ and $O_3$ in winter in Eastern China

Volatile organic compounds (VOCs) act as fuels for atmospheric chemistry leading to particulate matter (PM) and ozone ($O_3$). This study intends to unravel this complex process by focusing on oxygenated organic molecules (OOMs), which are key intermediates but still poorly understood. We found that OOMs are produced from anthropogenic VOC oxidation and interacted strongly with nitrogen oxides in winter in Eastern China. Importantly, the production of OOMs and their corresponding contributions to aerosol are amplified during photochemical haze when PM and $O_3$ are co-enhanced.

## As featured in:

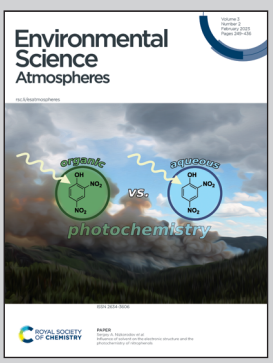


See Wei Nie *et al.*, *Environ. Sci.: Atmos.*, 2023, **3**, 282.

ROYAL SOCIETY OF CHEMISTRY

rsc.li/esatmospheres

Registered charity number: 207890

Environmental Science: Atmospheres

ROYAL SOCIETY OF CHEMISTRY

PAPER

View Article Online
View Journal | View Issue



Cite this: *Environ. Sci.: Atmos.*, 2023, **3**, 282

# Exploring condensable organic vapors and their co-occurrence with $PM_{2.5}$ and $O_3$ in winter in Eastern China†

Yuliang Liu, ‡[ab] Chong Liu,‡[ab] Wei Nie, *[ab] Yuanyuan Li,[ab] Dafeng Ge,[ab] Liangduo Chen,[ab] Caijun Zhu,[ab] Lei Wang,[ab] Yuxuan Zhang,[ab] Tengyu Liu, [ab] Ximeng Qi,[ab] Jiaping Wang,[ab] Dandan Huang,[c] Zhe Wang, [d] Chao Yan,[ab] Xuguang Chi[ab] and Aijun Ding[ab]

Oxygenated organic molecules (OOMs) are important oxidation products of volatile organic compounds (VOCs), and they act as key condensable vapors for new particle formation (NPF) and secondary organic aerosol (SOA) in the atmosphere. However, the large diversity and extremely low concentration make OOMs unmeasurable by conventional means, resulting in a poor understanding of OOMs, especially their formation. Herein, we observed OOMs with state-of-the-art mass spectrometry in a megacity in eastern China during the winter and characterized them by performing positive matrix factorization on binned mass spectra (binPMF). The binPMF analysis revealed 3 factors with clear precursor profiles (1 aromatic and 2 aliphatics), 2 ozone-related factors, 2 mixed-precursor-derived factors with unclear processes, and 4 factors dominated by nitrated phenols. We performed peak assignment on binPMF factors and identified over 1500 molecules with a mean total concentration of $4.7 \times 10^7$ molecules per $cm^3$ with all nitrated phenols excluded. Most OOMs are organic nitrates produced by the oxidation of anthropogenic VOC with interactions between the derived $RO_2$ and $NO_x$. These molecules containing 3 to 7 effective oxygen atoms (excluding $-NO_2$ in the nitrate moiety) introduced by autoxidation and multigenerational oxidation are less volatile, and hence, are susceptible to condensational loss. However, the observed OOM concentrations increase with the buildup of $PM_{2.5}$. This can be explained by enhanced OOM photochemical production owing to accumulated VOCs and sustained oxidants that outcompete condensational loss. This suggests favored SOA production *via* OOM condensation during haze. Furthermore, the highest OOM concentrations occur when $PM_{2.5}$ and $O_3$ are coenhanced. Under this condition, OOMs mainly come from ozone-related factors that are generated jointly with ozone and from aliphatic-dominated factors that are closely associated with $PM_{2.5}$. Overall, our results improve the understanding of OOM formation and its impact on the polluted atmosphere.

Received 30th October 2022
Accepted 4th January 2023

DOI: 10.1039/d2ea00143h

rsc.li/esatmospheres

## Environmental significance

Atmospheric secondary organic aerosols, whose precursors are volatile organic compounds, significantly affect climate forcing and human health. The discovery of oxygenated organic molecules (OOMs), which act as crucial intermediates, provides an opportunity to understand organic gas oxidation and aerosol formation at the molecular level. However, comprehensive elucidation of the nature and formation of OOMs is far from achieved, particularly in densely populated areas suffering from severe air pollution. Herein, we investigated wintertime OOMs observed using advanced mass spectrometry in a typical urban environment. We found that OOMs are produced from anthropogenic organic gas oxidation and interacted strongly with nitrogen oxides. Importantly, the photochemical production of OOMs and their corresponding contributions to aerosol are amplified during haze. Some characteristic OOM formation processes are linked to the simultaneous enhancement of $PM_{2.5}$ and ozone.

[a]*Joint International Research Laboratory of Atmospheric and Earth System Research, School of Atmospheric Sciences, Nanjing University, Nanjing, China. E-mail: niewei@nju.edu.cn*

[b]*National Observation and Research Station for Atmospheric Processes and Environmental Change in Yangtze River Delta, Nanjing, Jiangsu Province, China*

[c]*State Environmental Protection Key Laboratory of Formation and Prevention of Urban Air Pollution Complex, Shanghai Academy of Environmental Sciences, Shanghai, China*

[d]*Division of Environment and Sustainability, The Hong Kong University of Science and Technology, Hong Kong SAR, China*

† Electronic supplementary information (ESI) available. See DOI: https://doi.org/10.1039/d2ea00143h

‡ These authors contributed equally to this work.

# 1 Introduction

Secondary organic aerosol (SOA) is a ubiquitous and important component of atmospheric submicron particles,[1] which deteriorate air quality,[2,3] endanger human health[4] and affect the earth's radiation balance.[5] The oxidation of volatile organic compounds (VOCs) from anthropogenic and biogenic emissions ultimately leads to the formation of SOA,[6,7] with oxygenated organic molecules (OOMs)[8–10] being key intermediates in this convoluted process. Unlike traditional oxygenated VOCs, OOMs discovered using the latest developed mass spectrometric techniques[11–13] are a subset of VOC oxidation products attaining multiple oxygenated functionalities; thus, they are considerably less volatile than their precursors. Generally, OOMs belonging to ultra-low-volatility VOC (ULVOC) can participate in particle nucleation (~1 nm);[14,15] OOMs belonging to extremely-low-volatility (ELVOC) can drive the initial growth (1–3 nm);[16] and OOMs belonging to low-volatility VOC (LVOC) dominate the subsequent growth (3 to >50 nm).[8] When particles contain organic components, OOMs belonging to semi-volatile VOC (SVOC) can partition into the particle phase. All these processes are responsible for SOA formation.[17,18]

Currently, the formation of OOMs remains elusive.[9] Conventional VOC oxidation mechanisms[19] cannot account for OOMs with high O/C ratios. New ideas, including the autoxidation of organic peroxy radicals ($RO_2$),[20,21] dimerization of $RO_2$,[22] and multigenerational oxidation,[23,24] have recently been proposed as efficient ways to produce these condensable organic vapors. However, the formation of OOMs in the atmosphere is expected to be an integrated result of numerous known and unknown processes, which are extremely complex and of high variability at different spatiotemporal scales. Thus, comprehensive field investigations are warranted to elucidate the origins, formation, and compositions of OOMs in diverse ambient environments.

In general, the concentration of atmospheric OOMs is extremely low (dozens ppqv to dozens pptv),[25] making it difficult to detect. This leads to a scarcity of global observations of OOMs. Ambient OOM measurements were initially conducted in clean environments, such as forested or remote areas,[26–29] and later sporadically in anthropogenically polluted regions.[10,30,31] Moreover, many studies have focused on evaluating the contribution of OOMs to new particle formation (NPF) and SOA,[26,32,33] whereas only few studies have specifically investigated OOM sources. Ozonolysis and OH-initiated oxidation of monoterpenes are considered to be the main sources of OOMs in the boreal forest.[34,35] Isoprene and monoterpenes are identified as the main precursors of OOMs in the Southeastern US forest, and their oxidations are moderately influenced by anthropogenic emissions.[36] Instead, OOMs are found to be dominantly generated from the oxidation processes of anthropogenic VOCs under the strong perturbation of nitrogen oxides ($NO_x$) in urban cluster areas of eastern China.[37,38] These limited observations have significantly improved our understanding of OOMs, but the properties and formation of OOMs in the polluted atmosphere are not sufficiently addressed and are the focus of this study.

The Yangtze River Delta (YRD) region in eastern China, as a global hotspot for anthropogenic emissions, suffers from severe air pollution.[39,40] Although air pollution has been dramatically mitigated in recent years,[41,42] fine particulate matter ($PM_{2.5}$) and ozone ($O_3$) pollution remain major challenges for continuously improving air quality in this region.[43–45] Many studies have aimed to elucidate the scientific fundamentals behind the coordinated control of these two pollutants from the perspective of precursors ($NO_x$ and VOCs). It is noteworthy that OOMs are involved in chemical processes, resulting in $PM_{2.5}$ and $O_3$ pollution. Generally, VOCs are oxidized to produce $RO_2$, which convert NO to $NO_2$ and subsequently produce $O_3$ by $NO_2$ photolysis, meanwhile, $RO_2$ is terminated to form OOMs and then accumulate SOA by gas-particle partitioning.

In this study, we report a comprehensive analysis to ascertain the formation of OOMs during winter in Nanjing, a megacity in the YRD region. OOMs were observed using a chemical ionization atmospheric pressure interface time-of-flight mass spectrometer with nitrate reagent ions (nitrate CI-APi-TOF).[12] The characteristics of OOM sources or processes were explored by performing positive matrix factorization (PMF) on binned mass spectrometry data.[46,47] Then, the concentration, molecular composition, and volatility of the OOMs were investigated in detail. Finally, the connections of OOM formation with $PM_{2.5}$ and $O_3$ were discussed prospectively.

# 2 Methodology

## 2.1 Study site

The measurement was conducted at the Station for Observing Regional Processes of the Earth System (SORPES; 32°07′14″ N, 118°57′10″ E; 62 m a.s.l.)[48] from November 28, 2020 to January 3, 2021. The SORPES station is located in the northeastern suburbs of Nanjing, a megacity in the YRD region of eastern China. The station captures urban-scale emission activity[49] and is frequently impacted by polluted air masses from the North China Plain and the YRD urban agglomeration.[40,50] Detailed descriptions of the station can be found in previous studies.[51–55]

## 2.2 Instrumentation

A chemical ionization atmospheric pressure interface time-of-flight mass spectrometer with nitrate reagent ions (nitrate CI-APi-TOF; Aerodyne Research Inc. and Tofwerk AG) was used to detect ambient sulfuric acid and OOMs. The working principle[2,13] and sampling configuration[37] of this instrument were described in previous studies. Because standards for OOM measurable by the nitrate CI-APi-TOF are yet to be established, the concentrations of OOMs were quantified by an empirical method as described below:[15,16,56]

$$[\mathrm{OOM_i}] = \ln\left(1 + \frac{\sum_{n=0}^{1}\left[\mathrm{OOM_i}\cdot(\mathrm{HNO_3})_n\cdot\mathrm{NO_3}^- + (\mathrm{OOM_i}-\mathrm{H})^-\right]}{\sum_{n=0}^{2}\left[(\mathrm{HNO_3})_n\cdot\mathrm{NO_3}^-\right]}\right)\times C\times T_i. \quad (1)$$

Here, [$OOM_i$] is the concentration (molecules per $cm^3$) of an individual OOM. On the right-hand side of the equation, first, the numerator in parentheses is the detected total signals of an OOM charged in adduct-forming or deprotonated ways, and the denominator is the sum of all nitrate ion signals; both are in the unit of ions per s. Second, $C$ is an $H_2SO_4$-based calibration factor, determined as $6.0 \times 10^9$ molecules per $cm^3$ following the method of Kuerten *et al.*[57] Third, $T_i$ is a mass-dependent transmission efficiency inferred by depleting reagent ions with several perfluorinated acids.[58] Although calibration using this method leads to a lower limit estimate for the concentration of OOMs, especially for those with fewer oxygen atoms,[8,16] it is currently the most feasible method for quantifying the full spectrum of OOMs, and the uncertainty in this quantification does not subvert our conclusions.

VOCs were detected by applying a proton transfer reaction time-of-flight mass spectrometer (PTR-TOF-MS, Ionicon Analytik). $PM_{2.5}$ was measured using a combined technique of light scattering photometry and beta radiation attenuation (Thermo Scientific SHARP Monitor Model 5030). The chemical compositions of $PM_{2.5}$ were obtained from a time-of-flight aerosol chemical speciation monitor (TOF-ACSM, Aerodyne Research Inc.). The number of concentrations of particles was measured using a differential mobility particle spectrometer (DMPS), covering a size range from 6 to 800 nm. Trace gases, including $NO_x$, $NO_y$, $O_3$, $SO_2$ and CO, were monitored by applying Thermo Environmental Instruments (Models 42i-TL, 42i-Y, 49i, 43i-TLE, and API T300, respectively). $J(O^1D)$ was measured using an ultrafast CCD detector spectrometer, UVB enhanced (Meteorologieconsult Gmbh, Germany). Meteorological parameters were recorded by the Automatic Weather Station (CAMPEEL Co., AG1000).

### 2.3 BinPMF analysis

Positive matrix factorization (PMF)[59] was applied to binned mass spectra (binPMF[46]) to separate various sources or processes related to OOMs. Briefly, the raw mass spectra were divided into narrow bins with a width of 0.006 Th after mass calibration. Then, the PMF model inputs, including data and error matrices, were prepared based on an idea from Zhang *et al.*[46] The binPMF can separate the complex overlapping peaks and retain high resolution (HR) information as much as possible. This can minimize the uncertainty of HR peak fitting affecting the interpretation of PMF solutions. The PMF analysis in this study uses the IGOR-based analyzing interface SoFi (solution finder, version 6.8) and ME-2.[60] Details of the preparation and diagnostics of binPMF are provided in Section S2 in the ESI.†

## 3 Results and discussions

The observations were conducted during winter (low temperature and low radiation, as shown in Fig. S1† and 1a, respectively) with intensive anthropogenic emissions and their resulting aerosol pollution (Fig. S1† and 1b). The OOMs unambiguously exhibited time-dependent mass spectra and concentration

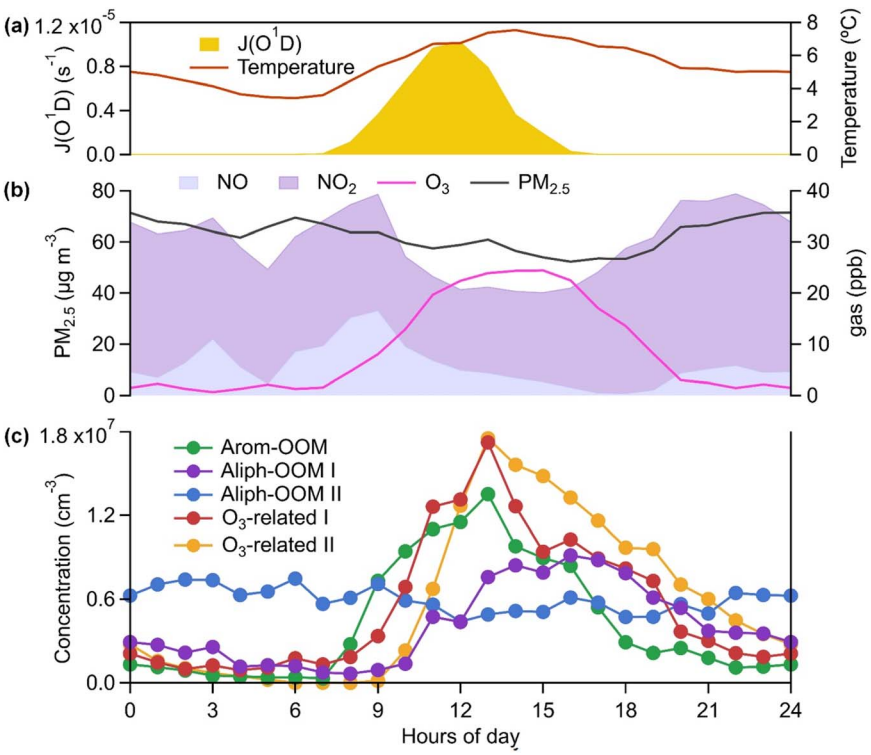


Fig. 1 Median diurnal variations of main compounds and parameters. (a) NO, $NO_2$, $O_3$, and $PM_{2.5}$. (b) $J(O^1D)$ and temperature. (c) The Arom-OOM, Aliph-OOM-I, Aliph-OOM-II, $O_3$-related-I, and $O_3$-related-II factors from binPMF analysis to OOMs.

differences (Fig. S1†). To deconvolute the complex dynamic processes of OOM formation, we performed a binPMF analysis and found that the 13-factor solution could explain the data variation (Fig. S5 and S6†). The selected solution includes 3 factors from the oxidation of a single anthropogenic VOC family (Fig. 1c), 2 factors related to ozone chemistry (Fig. 1c), 2 factors derived from mixed precursors with unclear processes (Fig. S14†), 4 factors dominated by nitrated phenols (NPs, Fig. S17†) and 2 factors dominated by fluorinated contaminations. NPs that are usually volatile have been broadly investigated.[61–64] Fluorinated contaminations come from Teflon tube volatiles and perfluoric acid for transmission efficiency calibrations. These two types of compounds are not our concern. The other 7 factors are dominated by organic nitrates (Fig. 2 and S14†), which are expected to contribute significantly to the particulate organic nitrates observed at this site.[65] Detailed discussions of these OOM factors are given below (Table 1).

### 3.1 Anthropogenic VOC chemistry

The first three factors possess clear anthropogenic precursor features, including one mainly from the oxidation of aromatic VOCs (denoted as Arom-OOM) and the other two from the oxidation of aliphatic VOCs (Aliph-OOMs I and II). The Arom-OOM factor is characterized by molecules with a double bond equivalent (DBE) of 3 (Fig. 2a), in which the most prominent ones are $C_xH_{2x-5}O_6N$ ($x = [6, 12]$, Table S2†). They are produced from the reactions of a homologous series of OH-initiated

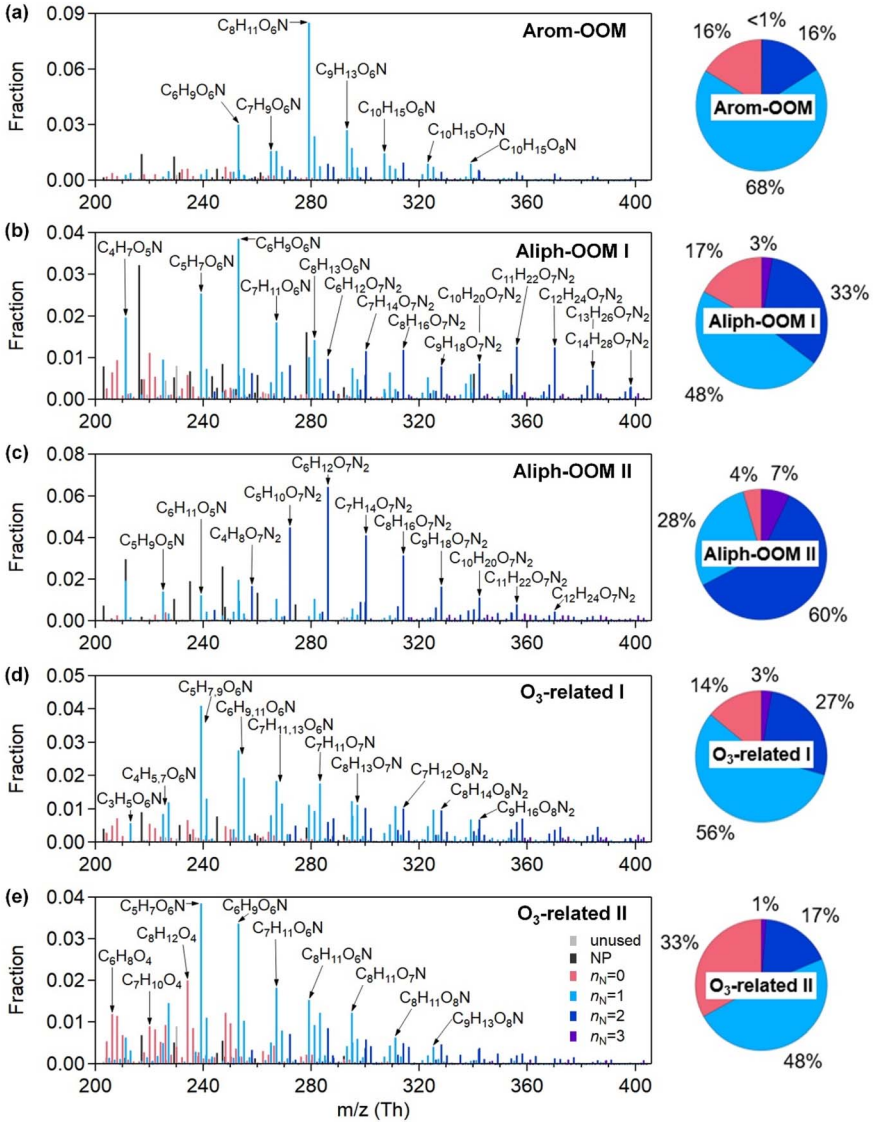


Fig. 2 Profiles of 5 binPMF factors. Mass spectra of (a) the Arom-OOM factor, (b) the Aliph-OOM-I factor, (c) the Aliph-OOM-II factor, (d) the $O_3$-related-I factor, and (e) the $O_3$-related-II factor. The elemental formulae of the major peaks are labeled above them. Peaks are color-coded by $n_N$, and the fractions of peaks grouped by $n_N$ are reported in the pie chart for each factor. The gray sticks are fluorinated contaminations or non-identified compounds. The nitrated phenols are drawn separately with black peaks. Therefore, $n_N$ can more reliably represent the number of nitrate groups in each molecule.

Table 1 Summary of molecular characteristics of 7 discussed non-nitrated-phenol factors. The calculation of the relevant parameters is given in Section S3 in the ESI. The major peaks of each factor are summarized in Section S4 in the ESI[a]

| Factor | Average concentration ($cm^{-3}$) | Effective formulas | MW ($g\ mol^{-1}$) | OSc | O : C | N : C | DBE | $\log_{10}(C^*(\mu g\ m^{-3}))$ in 300 K |
|---|---|---|---|---|---|---|---|---|
| Arom-OOM | $6.70 \times 10^6$ | $C_{8.4}H_{13.4}O_{6.1}N_{1.0}$ | 226.0 | −0.68 | 0.78 | 0.13 | 2.2 | 0.9 |
| Aliph-OOM I | $7.02 \times 10^6$ | $C_{8.2}H_{13.8}O_{6.2}N_{1.2}$ | 228.3 | −0.79 | 0.84 | 0.16 | 1.6 | 1.2 |
| Aliph-OOM II | $8.00 \times 10^6$ | $C_{7.4}H_{13.1}O_{6.9}N_{1.7}$ | 235.4 | −1.02 | 1.00 | 0.25 | 1.0 | 1.4 |
| $O_3$-related I | $8.01 \times 10^6$ | $C_{7.6}H_{11.9}O_{7.0}N_{1.2}$ | 232.5 | −0.40 | 0.99 | 0.17 | 2.1 | 0.5 |
| $O_3$-related II | $7.17 \times 10^6$ | $C_{7.0}H_{10.4}O_{6.1}N_{0.9}$ | 205.4 | −0.29 | 0.94 | 0.14 | 2.4 | 1.6 |
| MT-mixed-OOM | $6.19 \times 10^6$ | $C_{8.4}H_{13.4}O_{5.7}N_{1.0}$ | 219.6 | −0.77 | 0.74 | 0.13 | 2.2 | 1.3 |
| Mixed-OOM | $5.65 \times 10^6$ | $C_{7.4}H_{11.2}O_{5.8}N_{0.9}$ | 205.6 | −0.51 | 0.86 | 0.14 | 2.4 | 1.8 |

[a] MW is the molecular weight, OSc is the carbon oxidation state, O : C is the oxygen to carbon ratio, N : C is the nitrogen to carbon ratio, DBE is the double bond equivalent, $C^*$ the saturation concentration and $\log_{10}(C^*)$ is the volatility.

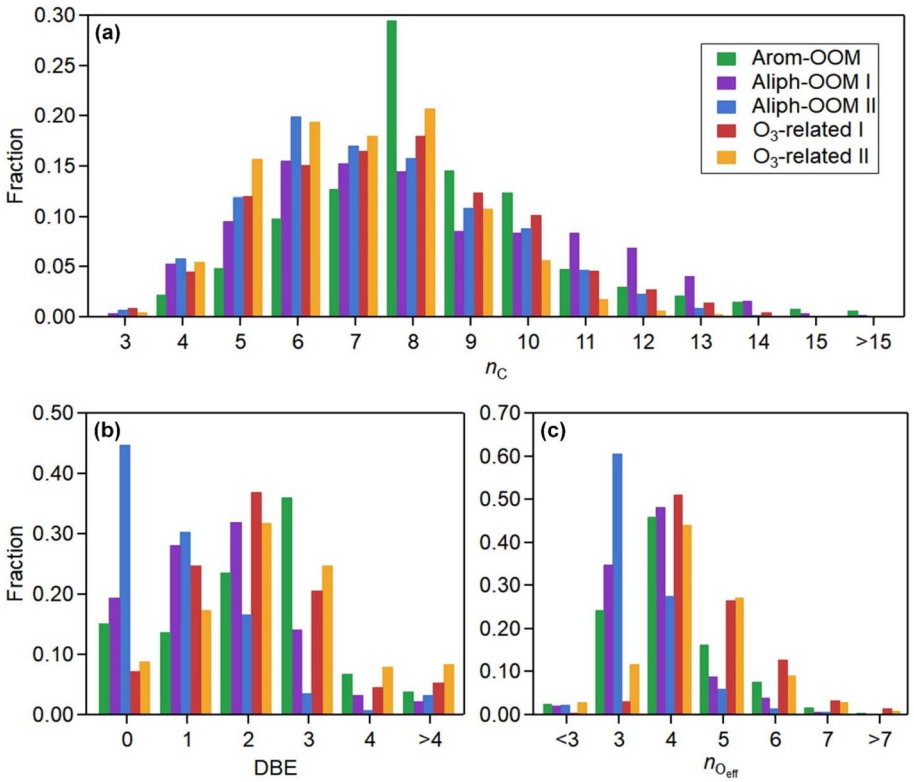


Fig. 3 The chemical distributions of 5 binPMF factors. The observed non-nitro OOMs grouped by (a) the number of carbon atoms ($n_C$), (b) DBE, and (c) the number of effective oxygen atoms ($n_{O_{eff}} = n_O - 2 \times n_N$), which exclude $-NO_2$ from the nitrate moiety.

aromatic bicyclic peroxy radicals with NO.[66] $C_8$-OOMs are the most abundant in this factor (Fig. 3a), which coincides with the OH reactivity distribution of aromatics (Fig. S8a†). This factor has a positive correlation (Fig. 4) and similar daily variation (Fig. S8b†) with the proxies of aromatic photo-oxidation (aromatics × $J(O^1D)$), with its concentration reaching a peak plateau after 10:00 local time (LT), declining after 14:00 LT, and staying low throughout the night (Fig. 1c). The $C_xH_{2x-5}O_8N$ ($x$ = [7, 11]) series (Table S2†) potentially formed through autoxidation (Fig. S9†) is still easy to observe although the abundances of $NO_x$ measured here are significantly higher than the set conditions of previous laboratory studies.[67–69] In addition, products with DBE < 3 (Fig. 3b) in this factor are supposed to be produced by multigenerational OH oxidations. These pathways can efficiently make aromatic-derived OOMs more oxidized, but more studies are needed to clarify their persistence under such heavily polluted conditions.

Unlike the Arom-OOM factor, the two factors from aliphatic oxidation comprise more saturated compounds (Fig. 1b, c and 3b), particularly a series of multi-nitrates (Tables S3 and S4†), such as $C_xH_{2x-2}O_{7-8}N_2$ ($x$ = [5, 13]) and $C_xH_{2x}O_7N_2$ ($x$ = [4, 13]). In the case of alkane oxidation under high $NO_x$, one OH attack can only add one nitrate group or one carbonyl group to the product molecule (Fig. S10†). According to the method

 

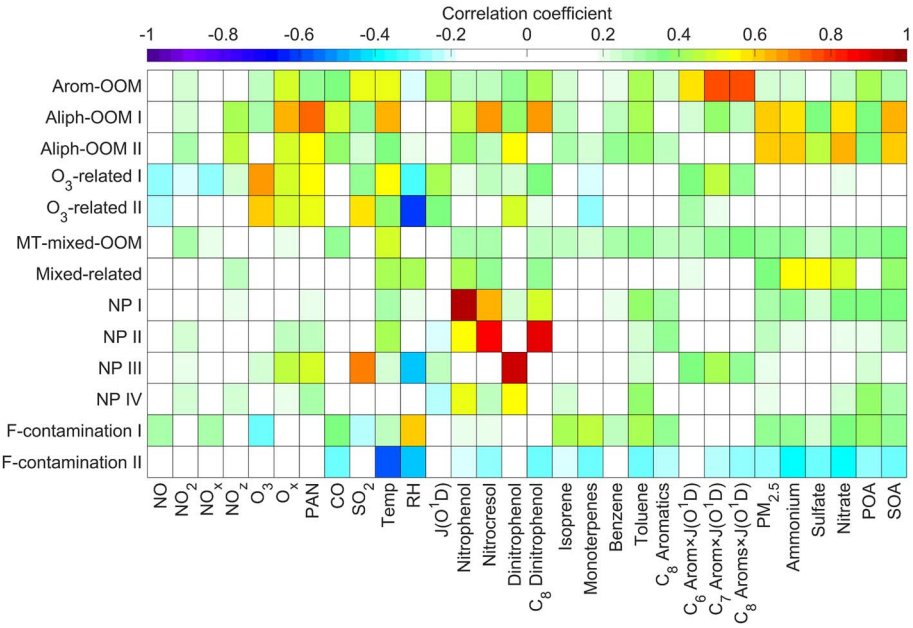


Fig. 4 Correlations of binPMF factors with external gas-phase and particulate tracers. The colors are differentiated by Pearson correlation coefficients. Note: $O_x$ is the total oxidants ($O_x = O_3 + NO_2 + NO_z$ and $NO_z = NO_y - NO_x$); aromatics × $J(O^1D)$ are the proxies of aromatic photooxidation; and primary and secondary organic aerosols (POA and SOA) are derived from PMF analysis of the organic aerosol detected by TOF-ACSM.

proposed by Liu *et al.*,[37] the two Aliph-OOM factors are dominated by second- and third-generation products (Fig. S10†). This observation validates the substantial amount of aliphatic dinitrates and trinitrates measured in recent laboratory experiments.[70,71] It seems that aromatic-derived OOMs contain more oxygen atoms than aliphatic-derived OOMs (Fig. 3c), and the latter are more prone to contain nitrate groups than the former (Fig. 1a–c). Thus, we speculate that aliphatics and aromatics play distinct roles in the budgets of reactive nitrogen oxides.[72]

Both Aliph-OOM factors are correlated with $PM_{2.5}$ (Fig. 4), suggesting their close connections with aerosol pollution. However, the two Aliph-OOM factors differ obviously in their temporal variation. The Aliph-OOM I factor has a later daytime peak (about 13:00–18:00 LT, Fig. 1c), suggesting that these multi-generational products are formed locally and require enough photochemistry. In contrast, the Aliph-OOM-II factor shows unclear diurnal variation (Fig. 1c) and presents many accumulation episodes in the time series, such as $PM_{2.5}$ (Fig. S1†). Thus, it is more likely to characterize OOMs in aged air masses transported to this site. The properties of OOMs from the two different processes described above are distinct. The Aliph-OOM-I factor has a larger proportion of heavy ($C_{10-14}$) molecules than the Aliph-OOM-II factor does (Fig. 3a), which is probably because long-chain aliphatic nitrates are less volatile and more easily consumed by condensation onto particle surfaces during transport. Moreover, the Aliph-OOM-I factor has a higher fraction of potential carbonyl groups (Fig. 3b), such as the $C_xH_{2x-3}O_6N$ ($x = [5, 13]$) series with a DBE of 2, while the Aliph-OOM-II factor has a higher proportion of nitrate groups (Fig. 2b and c), such as the $C_xH_{2x-1}O_{9-10}N_3$ ($x = [5, 10]$) series. Both carbonyl and nitrate moieties are vulnerable to loss through heterogeneous uptake on particles.[72,73] The difference in chemical composition between the two factors and their high concentration at high particle loadings may be attributed to their generation processes. Future laboratory studies are urgently needed to reveal the unknown part of aliphatic oxidation in a typical urban atmosphere.

### 3.2 Ozone-related chemistry

In contrast to the above factors distinguished by precursors, the following two factors are driven by photochemistry. The $O_3$-related I factor is well correlated with ozone and peroxyacetyl nitrate (PAN) in 17 ozone production cases (Fig. 5a and b). These cases are selected by the following criteria: (a) good correlation between $O_3$ and time ($r > 0.9$), *i.e.*, $O_3$ is continuously produced without substantial interruptions; (b) the maximum hourly $J(O^1D)$ for the day exceeds $1 \times 10^{-5}$ $s^{-1}$; and (c) the duration of the case exceeds 2 hours. It follows that this factor exhibiting significant daytime peaks (Fig. 1c) is likely produced jointly with ozone and PAN by tropospheric photochemistry involving VOCs and $NO_x$.[74] The fingerprint molecules of the $O_3$-related-I factor (Fig. 2d and Table S5†) are the $C_xH_{2x-3}O_6N$ ($x = [4, 12]$) and $C_xH_{2x-1}O_6N$ ($x = [4, 11]$) series, which presumably contain a peroxy-acyl-nitrate moiety but one more carbonyl or hydroxyl than PAN, respectively. The $O_3$-related I factor has the lowest volatility (Table 1), resulting from the outstanding proportion of OOMs with an effective oxygen number ($n_{O_{eff}} = n_O - 2 \times n_N$) over 4 (Fig. 3c). This indicates that this specific VOC oxidation process linked to ozone production facilitates the production of condensable organic vapors and, hence, the accumulation of SOA (Fig. S12†).

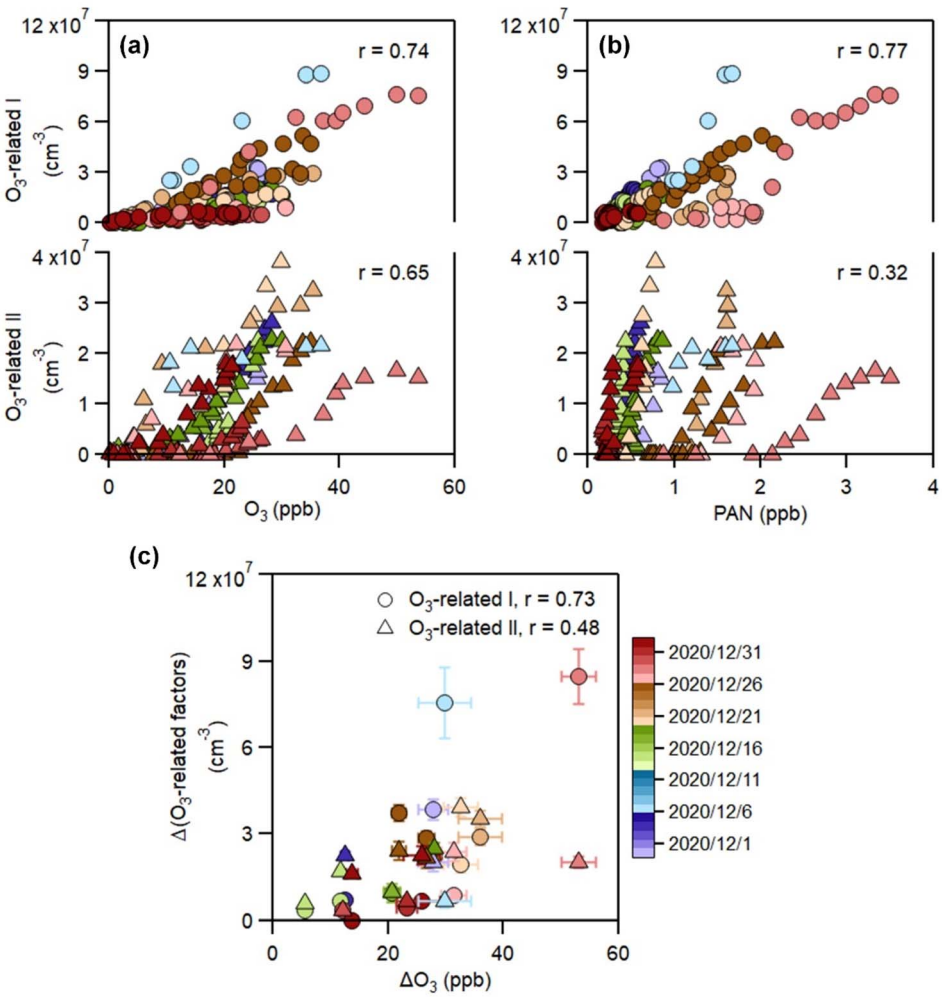


Fig. 5 Co-generation of the two $O_3$-related factors with ozone. Scatter plots of the two $O_3$-related factors with (a) ozone and (b) PAN in 17 ozone production cases. (c) Correlation between the increase in the two $O_3$-related factors and ozone. In 17 cases. Error bars indicate the statistical ($1\sigma$) uncertainties in fitting the ozone increase, and OOM increases during each case. All circles are colored by datetime to separate individual cases.

The $O_3$-related II factor, which is dominated by the $C_xH_{2x-3}O_6N$ ($x = [4, 10]$) and $C_xH_{2x-1}O_6N$ ($x = [4, 9]$) series (Fig. 2e and Table S6†), is moderately correlated with ozone and weakly correlated with PAN (Fig. 5a and b). This shows that the $O_3$-related II factor is partially homologous to the $O_3$-related-I factor. Both aliphatic-derived (DBE = 0, 1) and aromatic-derived OOMs (DBE = 3, 4) are present in these two factors (Fig. 3b), illustrating the crucial effect of anthropogenic VOCs on ozone production. Compared with the $O_3$-related-I factor, the $O_3$-related-II factor has a lower concentration in the morning (high NO) and a higher concentration in the afternoon (high temperature). Importantly, the $O_3$-related-II factor contains the most non-nitrates, which are related to chemical processes influenced by lower NO and higher temperature. It could be that the branching ratio of the $RO_2$ + NO reaction to nitrate decreases as the temperature increases,[72] or perhaps the contribution of the $RO_2$ + $HO_2$ reaction increases as NO decreases and temperature increases.[37]

### 3.3 Other OOM factors

Here are two OOM factors of mixed precursor origin without distinctive features. The MT-mixed-OOM factor contains potential monoterpene-derived OOMs (Fig. S14a†), such as $C_{10}H_{15,17}O_xN$ ($x = [5, 8]$) and $C_{10}H_{16}O_xN_2$ ($x = [7, 10]$). Monoterpenes are likely to stem from anthropogenic emissions in urban areas during the cold season,[75] and thus the co-presence of many oxidation products of anthropogenic precursors in this factor is understandable. The mixed-OOM factor comprising aliphatic-derived and aromatic-derived OOMs (Fig. S14b†) shows no clear relationship with the external gas-phase and particulate tracers (Fig. 4). It is noteworthy that these mixed factors cannot be further split by increasing the number of factors (Fig. S15 and S16†), indicating that they do not suffer from incomplete separations. Instead, they may come from complex nonlinear formation processes that are real in the atmosphere but cannot be interpreted well based on current understandings.

 

### 3.4 Connections of OOMs with $PM_{2.5}$ and $O_3$

Using binPMF to separate overlapping peaks and provide useful chemical information, over 1500 non-nitro molecules were identified through HR fitting and then reconstructed from the selected binPMF solution (Fig. S18a†). The mean total concentration is $4.7 \times 10^7$ molecules per $cm^3$, of which about 81% is organic nitrate generated by the reaction of $NO_x$ with $RO_2$ from anthropogenic-VOC oxidations (Fig. S18a†). Under such a strong influence of $NO_x$, non-nitro OOMs can still acquire 3–7 effective oxygen atoms (even over 7 for a few molecules) (Fig. S18b†), which benefit from multigenerational oxidation and autoxidation discussed in the aforementioned binPMF factors. Interestingly, the total OOM concentration is found to be correlated with $PM_{2.5}$ and $O_3$ (Fig. S19†). Understanding the formation of OOMs in relation to $PM_{2.5}$ and $O_3$ is an intriguing issue in the context of VOCs acting as fuels for atmospheric chemistry.[76]

First, the observed concentrations of OOMs from ELVOC to SVOC show unexpected upward trends with the accumulation of $PM_{2.5}$ (Fig. 6a). However, this suggests that OOM condensation (roughly represented by OOMs × CS, Fig. 6b) remains a crucial pathway of SOA formation during haze when the multiphase reactions are proposed to be significant.[2,73,77] This efficient gas-to-phase conversion has been revealed to be prevalent in major urban cluster areas in eastern China under highly polluted atmospheric conditions.[10] It is noteworthy that the percentage of SVOC in OOMs increases with $PM_{2.5}$ whereas the fractions of

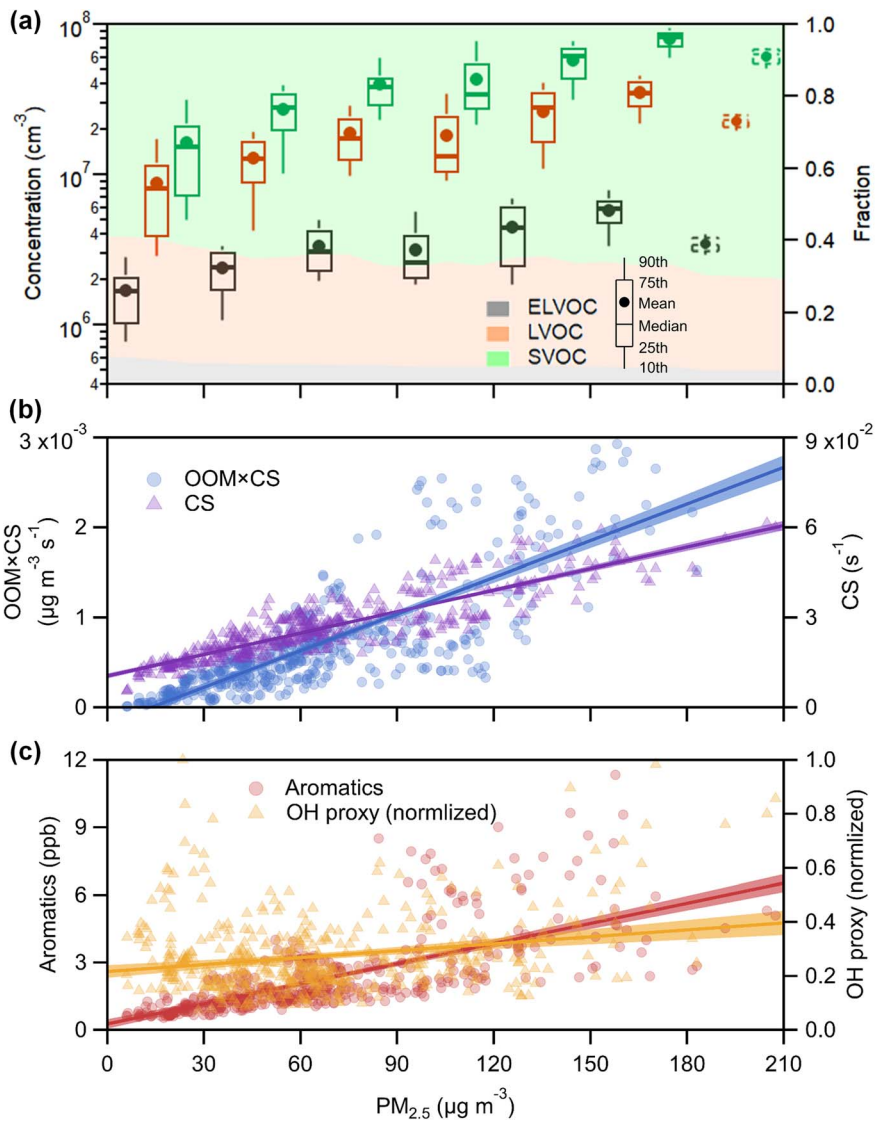


Fig. 6 The enhanced formation of OOMs during the haze (daytime). (a) Boxplots of the concentrations of OOMs (ELVOC, LVOC, and SVOC) binned by $PM_{2.5}$ in each 30 μg $m^{-3}$ interval of $PM_{2.5}$. All data for $PM_{2.5}$ > 180 μg $m^{-3}$ are represented by dashed box plots owing to too few data points. The relative contributions of ELVOC, LVOC, and SVOC for different $PM_{2.5}$ levels are displayed as color-filled areas. (b) Condensation sink (CS) and OOMs × CS roughly represent SOA production rate by OOM condensation, depending on $PM_{2.5}$. (c) Aromatics and OH proxy are accumulated with the increase of $PM_{2.5}$. All solid lines in (b) and (c) are obtained from the least squares linear fit, shaded with a 90% confidence interval.

ELVOC and LVOC decrease (Fig. 6a), which demonstrates that less volatile OOMs are more susceptible to condensation loss. However, the source of OOMs is supposed to increase much faster and outperforms the enhanced condensational loss of OOMs. With the buildup of haze, the emitted precursors (*e.g.*, aromatics) are enriched (Fig. 6c) owing to stagnant wind fields coupled with a shallow boundary layer.[78,79] At the high OH consumption rate induced by these reactive gases, the abundance of OH (represented by the OH proxy,[80] $\frac{[H_2SO_4] \times CS}{[SO_2]}$) does not decline (Fig. 6c) most likely owing to the rapid OH recycling from peroxyl radicals[81] and the atmospheric oxidation capability amplified by heterogeneous reactions on aerosol surfaces.[49,82,83] The intense photochemistry can also be deduced from the co-accumulation of PAN and $O_x$ with $PM_{2.5}$ (Fig. S20†). Consequently, the formation of OOMs and the contribution of OOMs to SOA are enhanced during haze (Fig. 6b).

Further, such strong photochemical production of OOMs is accompanied by efficient ozone production, which is usually masked by the fast removal caused by heavily emitted NO.[81] As shown in Fig. 7a, under moderate radiation conditions (the maximum daily $J(O^1D) > 1 \times 10^{-5}$ $s^{-1}$), the maximum daily 8 h average (MDA8) ozone follows 24 h average $PM_{2.5}$ and is elevated even on haze days. It has recently been found that ozone can benefit from active photochemistry to exceed the air quality standard during cold seasons in some areas with high VOC emissions[84,85] although ozone is generally considered to be a summertime pollutant.[86] Here, we pick three regimes on the scatter plot of MDA8 $O_3$ and 24 h average $PM_{2.5}$ (Fig. 7a) and then compare the formation of OOMs in different regimes

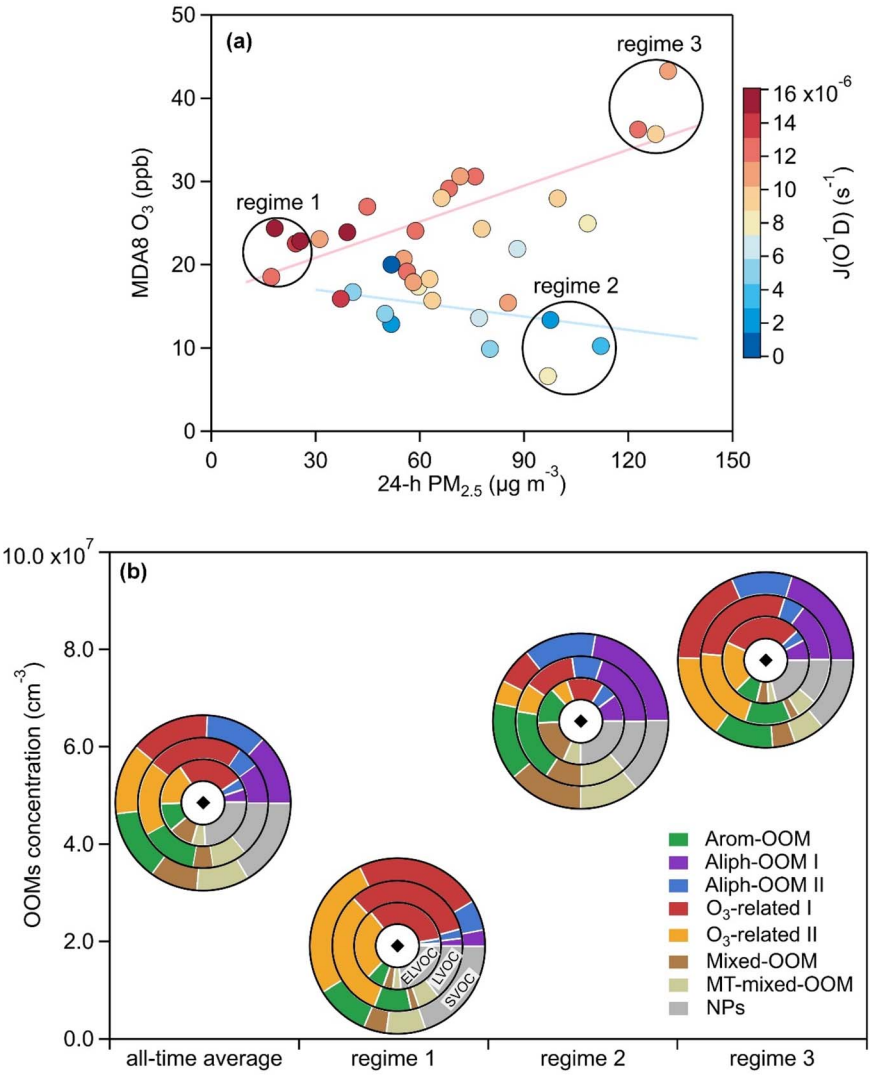


Fig. 7 The concurrence of OOMs with $PM_{2.5}$ and ozone. (a) Scatter plot of MDA8 $O_3$ with 24 h averaged $PM_{2.5}$. Each dot is colored by the maximum hourly $J(O^1D)$ of the corresponding day. Based on this chart, 3 regimes, including regime 1 (low 24 h average $PM_{2.5}$ and mid MDA8 $O_3$), regime 2 (high 24 h average $PM_{2.5}$ and low MDA8 $O_3$), and regime 3 (high 24 h average $PM_{2.5}$ and high MDA8 $O_3$), are determined. The light red solid line is obtained from the least squares linear fit in the case of $J(O^1D) > 1 \times 10^{-5}$ $s^{-1}$, and the light blue solid line is obtained in the case of $J(O^1D) < 0.8 \times 10^{-5}$ $s^{-1}$. (b) The contributions of binPMF factors to OOMs (ELVOC, LVOC, and SVOC) in all-time average and in 3 regimes. The total OOM concentration in different cases is given by solid black diamonds.

(Fig. 7b). Under relatively clean conditions (regime 1: low 24 h average $PM_{2.5}$ and mid MDA8 $O_3$), OOMs with different volatilities are mainly assigned to ozone-related factors (Fig. 7b). When shifting to normal winter haze conditions (regime 2: high 24 h average $PM_{2.5}$ and low MDA8 $O_3$), the major sources of OOMs are more extensive with clearly increased contributions from the two Aliph-OOM factors and the Arom-OOM factor (Fig. 7b), which ultimately increases OOM concentrations (Fig. 7b). The highest concentrations of OOMs are present in regime 3 (high 24 h average $PM_{2.5}$ and high MDA8 $O_3$) where OOMs are mainly sourced from ozone-related factors, followed by the Aliph-OOM factors (Fig. 7b). The role of VOC in $PM_{2.5}$ and $O_3$ pollution is usually interpreted based on traditional VOC oxidation mechanisms,[81,85] our analysis indicates that the perturbations introduced by the yet-to-be-resolved part of VOC oxidation (*i.e.*, formation of OOMs and organic nitrate) need to be addressed.

# 4 Summary and conclusions

We investigated the formation of gas-phase OOMs observed using a nitrate CI-APi-TOF in a megacity of eastern China during the winter. We performed binPMF analysis on the raw spectra. A high-quality OOM dataset containing over 1500 OOM molecules was established using binPMF to separate overlapping peaks. After excluding nitrated phenols, these OOMs have a mean total concentration of $4.7 \times 10^7$ molecules per $cm^3$, which predominantly comprised organic nitrate (~81% of the total), revealing the intense impact of $NO_x$ on the OOM formation. In addition, most OOMs contain 3 to 7 effective oxygen atoms owing to multigenerational oxidation and autoxidation, and their low-volatility feature favors SOA formation.

The binPMF analysis also identified 7 factors characterizing anthropogenic OOMs (excluding NPs). All factors mainly comprise homologous compounds because their precursors, anthropogenic VOCs, are usually co-emitted. Specifically, the Arom-OOM factor (peaking at 10:00–14:00 LT) is characterized by aromatic-derived unsaturated mononitrates, such as $C_xH_{2x-5}O_{6-8}N$ ($x = [6, 11]$). The Aliph-OOM-I factor (peaking at 13:00 to 18:00 LT) is dominated by aliphatic-derived nearly and fully saturated organic nitrates (mononitrates are the most abundant), such as $C_xH_{2x-1}O_{5,6}N$ ($x = [4, 12]$), $C_xH_{2x}O_7N_2$ ($x = [4, 14]$) and $C_xH_{2x-2}O_{7,8}N_2$ ($x = [6, 13]$). The Aliph-OOM-II factor, markedly affected by transport and associated with haze accumulation, comprises aliphatic-derived saturated and near-saturated organic nitrates (dinitrates are the most abundant), such as $C_xH_{2x}O_7N_2$ ($x = [4, 13]$), $C_xH_{2x-2}O_{7,8}N_2$ ($x = [5, 13]$), and $C_xH_{2x-1}O_{9,10}N_3$ ($x = [5, 10]$). The $O_3$-related-I factor (peaking around 13:00 LT), whose fingerprint molecules are $C_xH_{2x-3}O_6N$ ($x = [4, 12]$), is correlated with ozone and PAN; hence, it is suggested to be an important co-products with ozone from atmospheric photochemistry. The $O_3$-related-II factor (peaking around 13:00 LT) also correlates with ozone. In addition to sharing the same fingerprint molecules with the $O_3$-related-I factor, it contains the most abundant non-nitrates, such as $C_xH_{2x-4}O_{4,5}$ ($x = [5, 10]$), possibly derived from $RO_2$ terminations influenced by lower NO and higher temperature. The MT-mixed-OOM factor and the Mixed-OOM factor are derived from mixed precursors undergoing unknown processes. Notably, these characteristic profiles of OOMs have not been found in the available laboratory results and cannot be well explained by existing explicit chemical mechanisms. These observational findings can inform and inspire future laboratory and mechanistic studies of OOMs.

Finally, we analyzed the relationship of OOMs with $PM_{2.5}$ and $O_3$. As the condensation sink increases during the buildup of haze, the concentration of OOMs from ELVOC to SVOC shows an unexpected upward trend. This phenomenon illustrates that the VOC to SOA process is accelerated through OOM condensation and indicates the enhanced photochemical production of OOMs, which is powered by the accumulated precursors owing to limited air diffusion and sustained oxidants by rapid $HO_x$ ($OH + HO_2$) cycling and heterogeneous reactions. Moreover, the highest OOM concentrations occurred in the case of the co-enhancement of $PM_{2.5}$ and $O_3$, which is generally due to active photochemistry on haze days. In detail, this is presumably ascribed to the chemical processes characterized by ozone-related factors that boost both $O_3$ and low-volatility OOMs, as well as those represented by the Aliph-OOM factors that are tightly related to $PM_{2.5}$. More studies should be conducted to unravel the formation of OOMs and to complement the understanding of the role of VOC oxidation in $PM_{2.5}$ and ozone pollution from this perspective.

# Author contributions

AD, WN and Yuliang Liu designed the study. Yuliang Liu, CL, WN and CY analyzed the data. YL, CL and WN wrote the manuscript. Yuanyuan Li, DG, LC, CZ, LW, YZ, TL, XQ, JW and XC collected other research materials. All authors participated in the relevant scientific discussion and commented on the manuscript.

# Conflicts of interest

There are no conflicts to declare.

# Acknowledgements

We thank the tofTools team for providing programs for data analysis of mass spectrometry. This work was supported by the National Natural Science Foundation of China (NSFC) project (92044301, 42220104006, 41875175, 42075101 and 41975154), the Jiangsu Provincial Collaborative Innovation Center of Climate Change and the Fundamental Research Funds for the Central Universities.

# References

1 J. L. Jimenez, M. R. Canagaratna, N. M. Donahue, A. S. H. Prevot, Q. Zhang, J. H. Kroll, P. F. DeCarlo, J. D. Allan, H. Coe, N. L. Ng, A. C. Aiken, K. S. Docherty, I. M. Ulbrich, A. P. Grieshop, A. L. Robinson, J. Duplissy, J. D. Smith, K. R. Wilson, V. A. Lanz, C. Hueglin, Y. L. Sun,

J. Tian, A. Laaksonen, T. Raatikainen, J. Rautiainen, P. Vaattovaara, M. Ehn, M. Kulmala, J. M. Tomlinson, D. R. Collins, M. J. Cubison, E. J. Dunlea, J. A. Huffman, T. B. Onasch, M. R. Alfarra, P. I. Williams, K. Bower, Y. Kondo, J. Schneider, F. Drewnick, S. Borrmann, S. Weimer, K. Demerjian, D. Salcedo, L. Cottrell, R. Griffin, A. Takami, T. Miyoshi, S. Hatakeyama, A. Shimono, J. Y. Sun, Y. M. Zhang, K. Dzepina, J. R. Kimmel, D. Sueper, J. T. Jayne, S. C. Herndon, A. M. Trimborn, L. R. Williams, E. C. Wood, A. M. Middlebrook, C. E. Kolb, U. Baltensperger and D. R. Worsnop, Evolution of Organic Aerosols in the Atmosphere, *Science*, 2009, **326**, 1525–1529.

2 R. Zhang, G. Wang, S. Guo, M. L. Zamora, Q. Ying, Y. Lin, W. Wang, M. Hu and Y. Wang, Formation of Urban Fine Particulate Matter, *Chem. Rev.*, 2015, **115**, 3803–3855.

3 R. J. Huang, Y. L. Zhang, C. Bozzetti, K. F. Ho, J. J. Cao, Y. M. Han, K. R. Daellenbach, J. G. Slowik, S. M. Platt, F. Canonaco, P. Zotter, R. Wolf, S. M. Pieber, E. A. Bruns, M. Crippa, G. Ciarelli, A. Piazzalunga, M. Schwikowski, G. Abbaszade, J. Schnelle-Kreis, R. Zimmermann, Z. S. An, S. Szidat, U. Baltensperger, I. El Haddad and A. S. H. Prevot, High secondary aerosol contribution to particulate pollution during haze events in China, *Nature*, 2014, **514**, 218–222.

4 J. Lelieveld, J. S. Evans, M. Fnais, D. Giannadaki and A. Pozzer, The contribution of outdoor air pollution sources to premature mortality on a global scale, *Nature*, 2015, **525**, 367–371.

5 S. Szopa, V. Naik, B. Adhikary, P. Artaxo, T. Berntsen, W. D. Collins, S. Fuzzi, L. Gallardo, A. Kiendler-Scharr, Z. Klimont, H. Liao, N. Unger and P. Zanis, in *Climate Change 2021: The Physical Science Basis. Contribution of Working Group I to the Sixth Assessment Report of the Intergovernmental Panel on Climate Change*, ed. V. Masson-Delmotte, P. Zhai, A. Pirani, S. L. Connors, C. Péan, S. Berger, N. Caud, Y. Chen, L. Goldfarb, M. I. Gomis, M. Huang, K. Leitzell, E. Lonnoy, J. B. R. Matthews, T. K. Maycock, T. Waterfield, O. Yelekçi, R. Yu and B. Zhou, Cambridge University Press, Cambridge, United Kingdom and New York, NY, USA, 2021, pp. 817–922, DOI: **10.1017/9781009157896.008**.

6 M. Hallquist, J. C. Wenger, U. Baltensperger, Y. Rudich, D. Simpson, M. Claeys, J. Dommen, N. M. Donahue, C. George, A. H. Goldstein, J. F. Hamilton, H. Herrmann, T. Hoffmann, Y. Iinuma, M. Jang, M. E. Jenkin, J. L. Jimenez, A. Kiendler-Scharr, W. Maenhaut, G. McFiggans, T. F. Mentel, A. Monod, A. S. H. Prevot, J. H. Seinfeld, J. D. Surratt, R. Szmigielski and J. Wildt, The formation, properties and impact of secondary organic aerosol: current and emerging issues, *Atmos. Chem. Phys.*, 2009, **9**, 5155–5236.

7 P. J. Ziemann and R. Atkinson, Kinetics, products, and mechanisms of secondary organic aerosol formation, *Chem. Soc. Rev.*, 2012, **41**, 6582–6605.

8 M. Ehn, J. A. Thornton, E. Kleist, M. Sipila, H. Junninen, I. Pullinen, M. Springer, F. Rubach, R. Tillmann, B. Lee, F. Lopez-Hilfiker, S. Andres, I. H. Acir, M. Rissanen, T. Jokinen, S. Schobesberger, J. Kangasluoma, J. Kontkanen, T. Nieminen, T. Kurten, L. B. Nielsen, S. Jorgensen, H. G. Kjaergaard, M. Canagaratna, M. D. Maso, T. Berndt, T. Petaja, A. Wahner, V. M. Kerminen, M. Kulmala, D. R. Worsnop, J. Wildt and T. F. Mentel, A large source of low-volatility secondary organic aerosol, *Nature*, 2014, **506**, 476–479.

9 F. Bianchi, T. Kurten, M. Riva, C. Mohr, M. P. Rissanen, P. Roldin, T. Berndt, J. D. Crounse, P. O. Wennberg, T. F. Mentel, J. Wildt, H. Junninen, T. Jokinen, M. Kulmala, D. R. Worsnop, J. A. Thornton, N. Donahue, H. G. Kjaergaard and M. Ehn, Highly oxygenated organic molecules (HOM) from gas-phase autoxidation involving peroxy radicals: a key contributor to atmospheric aerosol, *Chem. Rev.*, 2019, **119**, 3472–3509.

10 W. Nie, C. Yan, D. D. Huang, Z. Wang, Y. Liu, X. Qiao, Y. Guo, L. Tian, P. Zheng, Z. Xu, Y. Li, Z. Xu, X. Qi, P. Sun, J. Wang, F. Zheng, X. Li, R. Yin, K. R. Dallenbach, F. Bianchi, T. Petäjä, Y. Zhang, M. Wang, M. Schervish, S. Wang, L. Qiao, Q. Wang, M. Zhou, H. Wang, C. Yu, D. Yao, H. Guo, P. Ye, S. Lee, Y. J. Li, Y. Liu, X. Chi, V.-M. Kerminen, M. Ehn, N. M. Donahue, T. Wang, C. Huang, M. Kulmala, D. Worsnop, J. Jiang and A. Ding, Secondary organic aerosol formed by condensing anthropogenic vapours over China's megacities, *Nat. Geosci.*, 2022, **15**, 255–261.

11 H. Junninen, M. Ehn, T. Petaja, L. Luosujarvi, T. Kotiaho, R. Kostiainen, U. Rohner, M. Gonin, K. Fuhrer, M. Kulmala and D. R. Worsnop, A high-resolution mass spectrometer to measure atmospheric ion composition, *Atmos. Meas. Tech.*, 2010, **3**, 1039–1053.

12 T. Jokinen, M. Sipila, H. Junninen, M. Ehn, G. Lonn, J. Hakala, T. Petaja, R. L. Mauldin III, M. Kulmala and D. R. Worsnop, Atmospheric sulphuric acid and neutral cluster measurements using CI-APi-TOF, *Atmos. Chem. Phys.*, 2012, **12**, 4117–4125.

13 B. H. Lee, F. D. Lopez-Hilfiker, C. Mohr, T. Kurtén, D. R. Worsnop and J. A. Thornton, An iodide-adduct high-resolution time-of-flight chemical-ionization mass spectrometer: application to atmospheric inorganic and organic compounds, *Environ. Sci. Technol.*, 2014, **48**, 6309–6317.

14 F. Riccobono, S. Schobesberger, C. E. Scott, J. Dommen, I. K. Ortega, L. Rondo, J. Almeida, A. Amorim, F. Bianchi, M. Breitenlechner, A. David, A. Downard, E. M. Dunne, J. Duplissy, S. Ehrhart, R. C. Flagan, A. Franchin, A. Hansel, H. Junninen, M. Kajos, H. Keskinen, A. Kupc, A. Kuerten, A. N. Kvashin, A. Laaksonen, K. Lehtipalo, V. Makhmutov, S. Mathot, T. Nieminen, A. Onnela, T. Petaja, A. P. Praplan, F. D. Santos, S. Schallhart, J. H. Seinfeld, M. Sipila, D. V. Spracklen, Y. Stozhkov, F. Stratmann, A. Tome, G. Tsagkogeorgas, P. Vaattovaara, Y. Viisanen, A. Vrtala, P. E. Wagner, E. Weingartner, H. Wex, D. Wimmer, K. S. Carslaw, J. Curtius, N. M. Donahue, J. Kirkby, M. Kulmala, D. R. Worsnop and U. Baltensperger, Oxidation products of biogenic emissions contribute to nucleation of atmospheric particles, *Science*, 2014, **344**, 717–721.

15 J. Kirkby, J. Duplissy, K. Sengupta, C. Frege, H. Gordon, C. Williamson, M. Heinritzi, M. Simon, C. Yan, J. Almeida, J. Trostl, T. Nieminen, I. K. Ortega, R. Wagner, A. Adamov, A. Amorim, A. K. Bernhammer, F. Bianchi, M. Breitenlechner, S. Brilke, X. M. Chen, J. Craven, A. Dias, S. Ehrhart, R. C. Flagan, A. Franchin, C. Fuchs, R. Guida, J. Hakala, C. R. Hoyle, T. Jokinen, H. Junninen, J. Kangasluoma, J. Kim, M. Krapf, A. Kurten, A. Laaksonen, K. Lehtipalo, V. Makhmutov, S. Mathot, U. Molteni, A. Onnela, O. Perakyla, F. Piel, T. Petaja, A. P. Praplan, K. Pringle, A. Rap, N. A. D. Richards, I. Riipinen, M. P. Rissanen, L. Rondo, N. Sarnela, S. Schobesberger, C. E. Scott, J. H. Seinfeld, M. Sipila, G. Steiner, Y. Stozhkov, F. Stratmann, A. Tome, A. Virtanen, A. L. Vogel, A. C. Wagner, P. E. Wagner, E. Weingartner, D. Wimmer, P. M. Winkler, P. L. Ye, X. Zhang, A. Hansel, J. Dommen, N. M. Donahue, D. R. Worsnop, U. Baltensperger, M. Kulmala, K. S. Carslaw and J. Curtius, Ion-induced nucleation of pure biogenic particles, *Nature*, 2016, **533**, 521–526.

16 J. Trostl, W. K. Chuang, H. Gordon, M. Heinritzi, C. Yan, U. Molteni, L. Ahlm, C. Frege, F. Bianchi, R. Wagner, M. Simon, K. Lehtipalo, C. Williamson, J. S. Craven, J. Duplissy, A. Adamov, J. Almeida, A. K. Bernhammer, M. Breitenlechner, S. Brilke, A. Dias, S. Ehrhart, R. C. Flagan, A. Franchin, C. Fuchs, R. Guida, M. Gysel, A. Hansel, C. R. Hoyle, T. Jokinen, H. Junninen, J. Kangasluoma, H. Keskinen, J. Kim, M. Krapf, A. Kurten, A. Laaksonen, M. Lawler, M. Leiminger, S. Mathot, O. Mohler, T. Nieminen, A. Onnela, T. Petaja, F. M. Piel, P. Miettinen, M. P. Rissanen, L. Rondo, N. Sarnela, S. Schobesberger, K. Sengupta, M. Sipila, J. N. Smith, G. Steiner, A. Tome, A. Virtanen, A. C. Wagner, E. Weingartner, D. Wimmer, P. M. Winkler, P. Ye, K. S. Carslaw, J. Curtius, J. Dommen, J. Kirkby, M. Kulmala, I. Riipinen, D. R. Worsnop, N. M. Donahue and U. Baltensperger, The role of low-volatility organic compounds in initial particle growth in the atmosphere, *Nature*, 2016, **533**, 527–531.

17 I. Riipinen, T. Yli-Juuti, J. R. Pierce, T. Petaja, D. R. Worsnop, M. Kulmala and N. M. Donahue, The contribution of organics to atmospheric nanoparticle growth, *Nat. Geosci.*, 2012, **5**, 453–458.

18 M. Kulmala, R. Cai, D. Stolzenburg, Y. Zhou, L. Dada, Y. Guo, C. Yan, T. Petäjä, J. Jiang and V.-M. Kerminen, The contribution of new particle formation and subsequent growth to haze formation, *Environ. Sci.: Atmos.*, 2022, **2**, 352–361.

19 M. E. Jenkin, J. C. Young and A. R. Rickard, The MCM v3.3.1 degradation scheme for isoprene, *Atmos. Chem. Phys.*, 2015, **15**, 11433–11459.

20 J. D. Crounse, L. B. Nielsen, S. Jørgensen, H. G. Kjaergaard and P. O. Wennberg, Autoxidation of organic compounds in the atmosphere, *J. Phys. Chem. Lett.*, 2013, **4**, 3513–3520.

21 T. Jokinen, M. Sipila, S. Richters, V. M. Kerminen, P. Paasonen, F. Stratmann, D. Worsnop, M. Kulmala, M. Ehn, H. Herrmann and T. Berndt, Rapid autoxidation forms highly oxidized $RO_2$ radicals in the atmosphere, *Angew. Chem., Int. Ed.*, 2014, **53**, 14596–14600.

22 J. J. Orlando and G. S. Tyndall, Laboratory studies of organic peroxy radical chemistry: an overview with emphasis on recent issues of atmospheric significance, *Chem. Soc. Rev.*, 2012, **41**, 6294–6317.

23 O. Garmash, M. P. Rissanen, I. Pullinen, S. Schmitt, O. Kausiala, R. Tillmann, D. Zhao, C. Percival, T. J. Bannan, M. Priestley, Å. M. Hallquist, E. Kleist, A. Kiendler-Scharr, M. Hallquist, T. Berndt, G. McFiggans, J. Wildt, T. F. Mentel and M. Ehn, Multi-generation OH oxidation as a source for highly oxygenated organic molecules from aromatics, *Atmos. Chem. Phys.*, 2020, **20**, 515–537.

24 M. Wang, D. Chen, M. Xiao, Q. Ye, D. Stolzenburg, V. Hofbauer, P. Ye, A. L. Vogel, R. L. Mauldin, A. Amorim, A. Baccarini, B. Baumgartner, S. Brilke, L. Dada, A. Dias, J. Duplissy, H. Finkenzeller, O. Garmash, X.-C. He, C. R. Hoyle, C. Kim, A. Kvashnin, K. Lehtipalo, L. Fischer, U. Molteni, T. Petäjä, V. Pospisilova, L. L. J. Quéléver, M. Rissanen, M. Simon, C. Tauber, A. Tomé, A. C. Wagner, L. Weitz, R. Volkamer, P. M. Winkler, J. Kirkby, D. R. Worsnop, M. Kulmala, U. Baltensperger, J. Dommen, I. El-Haddad and N. M. Donahue, Photo-oxidation of aromatic hydrocarbons produces low-volatility organic compounds, *Environ. Sci. Technol.*, 2020, **54**, 7911–7921.

25 Y. Guo, C. Yan, Y. Liu, X. Qiao, F. Zheng, Y. Zhang, Y. Zhou, C. Li, X. Fan, Z. Lin, Z. Feng, Y. Zhang, P. Zheng, L. Tian, W. Nie, Z. Wang, D. Huang, K. R. Daellenbach, L. Yao, L. Dada, F. Bianchi, J. Jiang, Y. Liu, V. M. Kerminen and M. Kulmala, Seasonal variation in oxygenated organic molecules in urban Beijing and their contribution to secondary organic aerosol, *Atmos. Chem. Phys.*, 2022, **22**, 10077–10097.

26 C. Mohr, J. A. Thornton, A. Heitto, F. D. Lopez-Hilfiker, A. Lutz, I. Riipinen, J. Hong, N. M. Donahue, M. Hallquist, T. Petäjä, M. Kulmala and T. Yli-Juuti, Molecular identification of organic vapors driving atmospheric nanoparticle growth, *Nat. Commun.*, 2019, **10**, 4442.

27 Q. Zha, C. Yan, H. Junninen, M. Riva, N. Sarnela, J. Aalto, L. Quéléver, S. Schallhart, L. Dada, L. Heikkinen, O. Peräkylä, J. Zou, C. Rose, Y. Wang, I. Mammarella, G. Katul, T. Vesala, D. R. Worsnop, M. Kulmala, T. Petäjä, F. Bianchi and M. Ehn, Vertical characterization of highly oxygenated molecules (HOMs) below and above a boreal forest canopy, *Atmos. Chem. Phys.*, 2018, **18**, 17437–17450.

28 F. Bianchi, J. Tröstl, H. Junninen, C. Frege, S. Henne, C. R. Hoyle, U. Molteni, E. Herrmann, A. Adamov, N. Bukowiecki, X. Chen, J. Duplissy, M. Gysel, M. Hutterli, J. Kangasluoma, J. Kontkanen, A. Kürten, H. E. Manninen, S. Münch, O. Peräkylä, T. Petäjä, L. Rondo, C. Williamson, E. Weingartner, J. Curtius, D. R. Worsnop, M. Kulmala, J. Dommen and U. Baltensperger, New particle formation in the free troposphere: A question of chemistry and timing, *Science*, 2016, **352**, 1109–1112.

29 F. Bianchi, H. Junninen, A. Bigi, V. A. Sinclair, L. Dada, C. R. Hoyle, Q. Zha, L. Yao, L. R. Ahonen, P. Bonasoni,

S. Buenrostro Mazon, M. Hutterli, P. Laj, K. Lehtipalo, J. Kangasluoma, V. M. Kerminen, J. Kontkanen, A. Marinoni, S. Mirme, U. Molteni, T. Petäjä, M. Riva, C. Rose, K. Sellegri, C. Yan, D. R. Worsnop, M. Kulmala, U. Baltensperger and J. Dommen, Biogenic particles formed in the Himalaya as an important source of free tropospheric aerosols, *Nat. Geosci.*, 2021, **14**, 4–9.

30 X. Qiao, C. Yan, X. Li, Y. Guo, R. Yin, C. Deng, C. Li, W. Nie, M. Wang, R. Cai, D. Huang, Z. Wang, L. Yao, D. R. Worsnop, F. Bianchi, Y. Liu, N. M. Donahue, M. Kulmala and J. Jiang, Contribution of Atmospheric Oxygenated Organic Compounds to Particle Growth in an Urban Environment, *Environ. Sci. Technol.*, 2021, **55**(2), 13646–13656.

31 C. Ye, B. Yuan, Y. Lin, Z. Wang, W. Hu, T. Li, W. Chen, C. Wu, C. Wang, S. Huang, J. Qi, B. Wang, C. Wang, W. Song, X. Wang, E. Zheng, J. E. Krechmer, P. Ye, Z. Zhang, X. Wang, D. R. Worsnop and M. Shao, Chemical characterization of oxygenated organic compounds in the gas phase and particle phase using iodide CIMS with FIGAERO in urban air, *Atmos. Chem. Phys.*, 2021, **21**, 8455–8478.

32 Y. Wang, P. Clusius, C. Yan, K. Dällenbach, R. Yin, M. Wang, X.-C. He, B. Chu, Y. Lu, L. Dada, J. Kangasluoma, P. Rantala, C. Deng, Z. Lin, W. Wang, L. Yao, X. Fan, W. Du, J. Cai, L. Heikkinen, Y. J. Tham, Q. Zha, Z. Ling, H. Junninen, T. Petäjä, M. Ge, Y. Wang, H. He, D. R. Worsnop, V.-M. Kerminen, F. Bianchi, L. Wang, J. Jiang, Y. Liu, M. Boy, M. Ehn, N. M. Donahue and M. Kulmala, Molecular Composition of Oxygenated Organic Molecules and Their Contributions to Organic Aerosol in Beijing, *Environ. Sci. Technol.*, 2022, **56**, 770–778.

33 X. Li, Y. Li, R. Cai, C. Yan, X. Qiao, Y. Guo, C. Deng, R. Yin, Y. Chen, Y. Li, L. Yao, N. Sarnela, Y. Zhang, T. Petäjä, F. Bianchi, Y. Liu, M. Kulmala, J. Hao, J. N. Smith and J. Jiang, Insufficient Condensable Organic Vapors Lead to Slow Growth of New Particles in an Urban Environment, *Environ. Sci. Technol.*, 2022, **56**, 9936–9946.

34 C. Yan, W. Nie, M. Äijälä, M. P. Rissanen, M. R. Canagaratna, P. Massoli, H. Junninen, T. Jokinen, N. Sarnela, S. A. K. Häme, S. Schobesberger, F. Canonaco, L. Yao, A. S. H. Prévôt, T. Petäjä, M. Kulmala, M. Sipilä, D. R. Worsnop and M. Ehn, Source characterization of highly oxidized multifunctional compounds in a boreal forest environment using positive matrix factorization, *Atmos. Chem. Phys.*, 2016, **16**, 12715–12731.

35 H. Y. Li, M. R. Canagaratna, M. Riva, P. Rantala, Y. J. Zhang, S. Thomas, L. Heikkinen, P. M. Flaud, E. Villenave, E. Perraudin, D. Worsnop, M. Kulmala, M. Ehn and F. Bianchi, Atmospheric organic vapors in two European pine forests measured by a Vocus PTR-TOF: insights into monoterpene and sesquiterpene oxidation processes, *Atmos. Chem. Phys.*, 2021, **21**, 4123–4147.

36 P. Massoli, H. Stark, M. R. Canagaratna, J. E. Krechmer, L. Xu, N. L. Ng, R. L. Mauldin III, C. Yan, J. Kimmel, P. K. Misztal, J. L. Jimenez, J. T. Jayne and D. R. Worsnop, Ambient Measurements of Highly Oxidized Gas-Phase Molecules during the Southern Oxidant and Aerosol Study (SOAS) 2013, *ACS Earth Space Chem.*, 2018, **2**, 653–672.

37 Y. Liu, W. Nie, Y. Li, D. Ge, C. Liu, Z. Xu, L. Chen, T. Wang, L. Wang, P. Sun, X. Qi, J. Wang, Z. Xu, J. Yuan, C. Yan, Y. Zhang, D. Huang, Z. Wang, N. M. Donahue, D. Worsnop, X. Chi, M. Ehn and A. Ding, Formation of condensable organic vapors from anthropogenic and biogenic volatile organic compounds (VOCs) is strongly perturbed by $NO_x$ in eastern China, *Atmos. Chem. Phys.*, 2021, **21**, 14789–14814.

38 Y. Zhang, D. Li, Y. Ma, C. Dubois, X. Wang, S. Perrier, H. Chen, H. Wang, S. a. Jing, Y. Lu, S. Lou, C. Yan, W. Nie, J. Chen, C. Huang, C. George and M. Riva, Field Detection of Highly Oxygenated Organic Molecules in Shanghai by Chemical Ionization–Orbitrap, *Environ. Sci. Technol.*, 2022, **56**, 7608–7617.

39 J. L. Hu, Y. G. Wang, Q. Ying and H. L. Zhang, Spatial and temporal variability of PM2.5 and PM10 over the North China Plain and the Yangtze River Delta, China, *Atmos. Environ.*, 2014, **95**, 598–609.

40 A. J. Ding, C. B. Fu, X. Q. Yang, J. N. Sun, L. F. Zheng, Y. N. Xie, E. Herrmann, W. Nie, T. Petäjä, V. M. Kerminen and M. Kulmala, Ozone and fine particle in the western Yangtze River Delta: an overview of 1 yr data at the SORPES station, *Atmos. Chem. Phys.*, 2013, **13**, 5813–5830.

41 Q. Zhang, Y. Zheng, D. Tong, M. Shao, S. Wang, Y. Zhang, X. Xu, J. Wang, H. He, W. Liu, Y. Ding, Y. Lei, J. Li, Z. Wang, X. Zhang, Y. Wang, J. Cheng, Y. Liu, Q. Shi, L. Yan, G. Geng, C. Hong, M. Li, F. Liu, B. Zheng, J. Cao, A. Ding, J. Gao, Q. Fu, J. Huo, B. Liu, Z. Liu, F. Yang, K. He and J. Hao, Drivers of improved PM2.5 air quality in China from 2013 to 2017, *Proc. Natl. Acad. Sci. U. S. A.*, 2019, **116**, 24463–24469.

42 A. Ding, X. Huang, W. Nie, X. Chi, Z. Xu, L. Zheng, Z. Xu, Y. Xie, X. Qi, Y. Shen, P. Sun, J. Wang, L. Wang, J. Sun, X.-Q. Yang, W. Qin, X. Zhang, W. Cheng, W. Liu, L. Pan and C. Fu, Significant reduction of PM2.5 in eastern China due to regional-scale emission control: evidence from SORPES in 2011–2018, *Atmos. Chem. Phys.*, 2019, **19**, 11791–11801.

43 K. Li, D. J. Jacob, H. Liao, J. Zhu, V. Shah, L. Shen, K. H. Bates, Q. Zhang and S. Zhai, A two-pollutant strategy for improving ozone and particulate air quality in China, *Nat. Geosci.*, 2019, **12**, 906–910.

44 H. Dai, J. Zhu, H. Liao, J. Li, M. Liang, Y. Yang and X. Yue, Co-occurrence of ozone and PM2.5 pollution in the Yangtze River Delta over 2013–2019: Spatiotemporal distribution and meteorological conditions, *Atmos. Res.*, 2021, **249**, 105363.

45 N. Wang, J. Xu, C. Pei, R. Tang, D. Zhou, Y. Chen, M. Li, X. Deng, T. Deng, X. Huang and A. Ding, Air Quality During COVID-19 Lockdown in the Yangtze River Delta and the Pearl River Delta: Two Different Responsive Mechanisms to Emission Reductions in China, *Environ. Sci. Technol.*, 2021, **55**, 5721–5730.

46 Y. Zhang, O. Peräkylä, C. Yan, L. Heikkinen, M. Äijälä, K. R. Daellenbach, Q. Zha, M. Riva, O. Garmash,

 

H. Junninen, P. Paatero, D. Worsnop and M. Ehn, A novel approach for simple statistical analysis of high-resolution mass spectra, *Atmos. Meas. Tech.*, 2019, **12**, 3761–3776.

47 Y. Zhang, O. Peräkylä, C. Yan, L. Heikkinen, M. Äijälä, K. R. Daellenbach, Q. Zha, M. Riva, O. Garmash, H. Junninen, P. Paatero, D. Worsnop and M. Ehn, Insights into atmospheric oxidation processes by performing factor analyses on subranges of mass spectra, *Atmos. Chem. Phys.*, 2020, **20**, 5945–5961.

48 A. Ding, W. Nie, X. Huang, X. Chi, J. Sun, V.-M. Kerminen, Z. Xu, W. Guo, T. Petäjä, X. Yang, M. Kulmala and C. Fu, Long-term observation of air pollution-weather/climate interactions at the SORPES station: a review and outlook, *Front. Environ. Sci. Eng.*, 2016, **10**, 15.

49 Y. Liu, W. Nie, Z. Xu, T. Wang, R. Wang, Y. Li, L. Wang, X. Chi and A. Ding, Semi-quantitative understanding of source contribution to nitrous acid (HONO) based on 1 year of continuous observation at the SORPES station in eastern China, *Atmos. Chem. Phys.*, 2019, **19**, 13289–13308.

50 X. M. Qi, A. J. Ding, W. Nie, T. Petäjä, V. M. Kerminen, E. Herrmann, Y. N. Xie, L. F. Zheng, H. Manninen, P. Aalto, J. N. Sun, Z. N. Xu, X. G. Chi, X. Huang, M. Boy, A. Virkkula, X. Q. Yang, C. B. Fu and M. Kulmala, Aerosol size distribution and new particle formation in the western Yangtze River Delta of China: 2 years of measurements at the SORPES station, *Atmos. Chem. Phys.*, 2015, **15**, 12445–12464.

51 J. Wang, W. Nie, Y. Cheng, Y. Shen, X. Chi, J. Wang, X. Huang, Y. Xie, P. Sun, Z. Xu, X. Qi, H. Su and A. Ding, Light absorption of brown carbon in eastern China based on 3-year multi-wavelength aerosol optical property observations and an improved absorption Ångström exponent segregation method, *Atmos. Chem. Phys.*, 2018, **18**, 9061–9074.

52 P. Sun, W. Nie, X. Chi, Y. Xie, X. Huang, Z. Xu, X. Qi, Z. Xu, L. Wang, T. Wang, Q. Zhang and A. Ding, Two years of online measurement of fine particulate nitrate in the western Yangtze River Delta: influences of thermodynamics and $N_2O_5$ hydrolysis, *Atmos. Chem. Phys.*, 2018, **18**, 17177–17190.

53 Y. Shen, A. Virkkula, A. Ding, J. Wang, X. Chi, W. Nie, X. Qi, X. Huang, Q. Liu, L. Zheng, Z. Xu, T. Petäjä, P. P. Aalto, C. Fu and M. Kulmala, Aerosol optical properties at SORPES in Nanjing, east China, *Atmos. Chem. Phys.*, 2018, **18**, 5265–5292.

54 L. Chen, X. Qi, W. Nie, J. Wang, Z. Xu, T. Wang, Y. Liu, Y. Shen, Z. Xu, T. V. Kokkonen, X. Chi, P. P. Aalto, P. Paasonen, V.-M. Kerminen, T. Petäjä, M. Kulmala and A. Ding, Cluster Analysis of Submicron Particle Number Size Distributions at the SORPES Station in the Yangtze River Delta of East China, *J. Geophys. Res.: Atmos.*, 2021, **126**, e2020JD034004.

55 Z. N. Xu, W. Nie, Y. L. Liu, P. Sun, D. D. Huang, C. Yan, J. Krechmer, P. L. Ye, Z. Xu, X. M. Qi, C. J. Zhu, Y. Y. Li, T. Y. Wang, L. Wang, X. Huang, R. Z. Tang, S. Guo, G. L. Xiu, Q. Y. Fu, D. Worsnop, X. G. Chi and A. J. Ding, Multifunctional products of isoprene oxidation in polluted atmosphere and their contribution to SOA, *Geophys. Res. Lett.*, 2021, **48**, e2020GL089276.

56 D. Stolzenburg, L. Fischer, A. L. Vogel, M. Heinritzi, M. Schervish, M. Simon, A. C. Wagner, L. Dada, L. R. Ahonen, A. Amorim, A. Baccarini, P. S. Bauer, B. Baumgartner, A. Bergen, F. Bianchi, M. Breitenlechner, S. Brilke, S. B. Mazon, D. Chen, A. Dias, D. C. Draper, J. Duplissy, I. El Haddad, H. Finkenzeller, C. Frege, C. Fuchs, O. Garmash, H. Gordon, X. He, J. Helm, V. Hofbauer, C. R. Hoyle, C. Kim, J. Kirkby, J. Kontkanen, A. Kuerten, J. Lampilahti, M. Lawler, K. Lehtipalo, M. Leiminger, H. Mai, S. Mathot, B. Mentler, U. Molteni, W. Nie, T. Nieminen, J. B. Nowak, A. Ojdanic, A. Onnela, M. Passananti, T. Petaja, L. L. J. Quelever, M. P. Rissanen, N. Sarnela, S. Schallhart, C. Tauber, A. Tome, R. Wagner, M. Wang, L. Weitz, D. Wimmer, M. Xiao, C. Yan, P. Ye, Q. Zha, U. Baltensperger, J. Curtius, J. Dommen, R. C. Flagan, M. Kulmala, J. N. Smith, D. R. Worsnop, A. Hansel, N. M. Donahue and P. M. Winkler, Rapid growth of organic aerosol nanoparticles over a wide tropospheric temperature range, *Proc. Natl. Acad. Sci. U. S. A.*, 2018, **115**, 9122–9127.

57 A. Kuerten, L. Rondo, S. Ehrhart and J. Curtius, Calibration of a chemical ionization mass spectrometer for the measurement of gaseous sulfuric acid, *J. Phys. Chem. A*, 2012, **116**, 6375–6386.

58 M. Heinritzi, M. Simon, G. Steiner, A. C. Wagner, A. Kuerten, A. Hansel and J. Curtius, Characterization of the mass-dependent transmission efficiency of a CIMS, *Atmos. Meas. Tech.*, 2016, **9**, 1449–1460.

59 P. Paatero and U. Tapper, Positive matrix factorization – a nonnegative factor model with optimal utilization of error-estimates of data values, *Environmetrics*, 1994, **5**, 111–126.

60 F. Canonaco, M. Crippa, J. G. Slowik, U. Baltensperger and A. S. H. Prévôt, SoFi, an IGOR-based interface for the efficient use of the generalized multilinear engine (ME-2) for the source apportionment: ME-2 application to aerosol mass spectrometer data, *Atmos. Meas. Tech.*, 2013, **6**, 3649–3661.

61 X. Cheng, Q. Chen, Y. Li, G. Huang, Y. Liu, S. Lu, Y. Zheng, W. Qiu, K. Lu, X. Qiu, F. Bianchi, C. Yan, B. Yuan, M. Shao, Z. Wang, M. R. Canagaratna, T. Zhu, Y. Wu and L. Zeng, Secondary production of gaseous nitrated phenols in polluted urban environments, *Environ. Sci. Technol.*, 2021, **55**, 4410–4419.

62 K. Song, S. Guo, H. Wang, Y. Yu, H. Wang, R. Tang, S. Xia, Y. Gong, Z. Wan, D. Lv, R. Tan, W. Zhu, R. Shen, X. Li, X. Yu, S. Chen, L. Zeng and X. Huang, Measurement report: Online measurement of gas-phase nitrated phenols utilizing a CI-LToF-MS: primary sources and secondary formation, *Atmos. Chem. Phys.*, 2021, **21**, 7917–7932.

63 Y. Chen, P. Zheng, Z. Wang, W. Pu, Y. Tan, C. Yu, M. Xia, W. Wang, J. Guo, D. Huang, C. Yan, W. Nie, Z. Ling, Q. Chen, S. Lee and T. Wang, Secondary Formation and Impacts of Gaseous Nitro-Phenolic Compounds in the

Continental Outflow Observed at a Background Site in South China, *Environ. Sci. Technol.*, 2021, **56**, 6933–6943.

64 C. Lu, X. Wang, J. Zhang, Z. Liu, Y. Liang, S. Dong, M. Li, J. Chen, H. Chen, H. Xie, L. Xue and W. Wang, Substantial emissions of nitrated aromatic compounds in the particle and gas phases in the waste gases from eight industries, *Environ. Pollut.*, 2021, **283**, 117132.

65 D. Ge, W. Nie, P. Sun, Y. Liu, T. Wang, J. Wang, J. Wang, L. Wang, C. Zhu, R. Wang, T. Liu, X. Chi and A. Ding, Characterization of particulate organic nitrates in the Yangtze River Delta, East China, using the time-of-flight aerosol chemical speciation monitor, *Atmos. Environ.*, 2022, **272**, 118927.

66 C. Bloss, V. Wagner, M. E. Jenkin, R. Volkamer, W. J. Bloss, J. D. Lee, D. E. Heard, K. Wirtz, M. Martin-Reviejo, G. Rea, J. C. Wenger and M. J. Pilling, Development of a detailed chemical mechanism (MCMv3.1) for the atmospheric oxidation of aromatic hydrocarbons, *Atmos. Chem. Phys.*, 2005, **5**, 641–664.

67 S. Wang, R. Wu, T. Berndt, M. Ehn and L. Wang, Formation of Highly Oxidized Radicals and Multifunctional Products from the Atmospheric Oxidation of Alkylbenzenes, *Environ. Sci. Technol.*, 2017, **51**, 8442–8449.

68 Y. Wang, A. Mehra, J. E. Krechmer, G. Yang, X. Hu, Y. Lu, A. Lambe, M. Canagaratna, J. Chen, D. Worsnop, H. Coe and L. Wang, Oxygenated products formed from OH-initiated reactions of trimethylbenzene: autoxidation and accretion, *Atmos. Chem. Phys.*, 2020, **20**, 9563–9579.

69 X. Cheng, Q. Chen, Y. Jie Li, Y. Zheng, K. Liao and G. Huang, Highly oxygenated organic molecules produced by the oxidation of benzene and toluene in a wide range of OH exposure and $NO_x$ conditions, *Atmos. Chem. Phys.*, 2021, **21**, 12005–12019.

70 D. S. Wang and L. Hildebrandt Ruiz, Chlorine-initiated oxidation of n-alkanes under high-$NO_x$ conditions: insights into secondary organic aerosol composition and volatility using a FIGAERO–CIMS, *Atmos. Chem. Phys.*, 2018, **18**, 15535–15553.

71 L. G. Jahn, D. S. Wang, S. V. Dhulipala and L. H. Ruiz, Gas-Phase Chlorine Radical Oxidation of Alkanes: Effects of Structural Branching, NOx, and Relative Humidity Observed during Environmental Chamber Experiments, *J. Phys. Chem. A*, 2021, **125**, 7303–7317.

72 A. E. Perring, S. E. Pusede and R. C. Cohen, An Observational Perspective on the Atmospheric Impacts of Alkyl and Multifunctional Nitrates on Ozone and Secondary Organic Aerosol, *Chem. Rev.*, 2013, **113**, 5848–5870.

73 V. F. McNeill, Aqueous Organic Chemistry in the Atmosphere: Sources and Chemical Processing of Organic Aerosols, *Environ. Sci. Technol.*, 2015, **49**, 1237–1244.

74 Y. Liu, H. Shen, J. Mu, H. Li, T. Chen, J. Yang, Y. Jiang, Y. Zhu, H. Meng, C. Dong, W. Wang and L. Xue, Formation of peroxyacetyl nitrate (PAN) and its impact on ozone production in the coastal atmosphere of Qingdao, North China, *Sci. Total Environ.*, 2021, **778**, 146265.

75 H. Wang, X. Ma, Z. Tan, H. Wang, X. Chen, S. Chen, Y. Gao, Y. Liu, Y. Liu, X. Yang, B. Yuan, L. Zeng, C. Huang, K. Lu and Y. Zhang, Anthropogenic monoterpenes aggravating ozone pollution, *Natl. Sci. Rev.*, 2022, **9**, nwac103.

76 C. L. Heald and J. H. Kroll, The fuel of atmospheric chemistry: Toward a complete description of reactive organic carbon, *Sci. Adv.*, 2020, **6**, eaay8967.

77 J. Wang, J. Ye, Q. Zhang, J. Zhao, Y. Wu, J. Li, D. Liu, W. Li, Y. Zhang, C. Wu, C. Xie, Y. Qin, Y. Lei, X. Huang, J. Guo, P. Liu, P. Fu, Y. Li, H. C. Lee, H. Choi, J. Zhang, H. Liao, M. Chen, Y. Sun, X. Ge, S. T. Martin and D. J. Jacob, Aqueous production of secondary organic aerosol from fossil-fuel emissions in winter Beijing haze, *Proc. Natl. Acad. Sci. U. S. A.*, 2021, **118**, e2022179118.

78 T. Petäjä, L. Järvi, V. M. Kerminen, A. J. Ding, J. N. Sun, W. Nie, J. Kujansuu, A. Virkkula, X. Yang, C. B. Fu, S. Zilitinkevich and M. Kulmala, Enhanced air pollution *via* aerosol-boundary layer feedback in China, *Sci. Rep.*, 2016, **6**, 18998.

79 A. J. Ding, X. Huang, W. Nie, J. N. Sun, V. M. Kerminen, T. Petäjä, H. Su, Y. F. Cheng, X. Q. Yang, M. H. Wang, X. G. Chi, J. P. Wang, A. Virkkula, W. D. Guo, J. Yuan, S. Y. Wang, R. J. Zhang, Y. F. Wu, Y. Song, T. Zhu, S. Zilitinkevich, M. Kulmala and C. B. Fu, Enhanced haze pollution by black carbon in megacities in China, *Geophys. Res. Lett.*, 2016, **43**, 2873–2879.

80 L. Yang, W. Nie, Y. Liu, Z. Xu, M. Xiao, X. Qi, Y. Li, R. Wang, J. Zou, P. Paasonen, C. Yan, Z. Xu, J. Wang, C. Zhou, J. Yuan, J. Sun, X. Chi, V.-M. Kerminen, M. Kulmala and A. Ding, Towards building a physical proxy for gas-phase sulfuric acid concentration based on its budget analysis in polluted Yangtze River Delta, east China, *Environ. Sci. Technol.*, 2021, **55**, 6665–6676.

81 K. Lu, H. Fuchs, A. Hofzumahaus, Z. Tan, H. Wang, L. Zhang, S. H. Schmitt, F. Rohrer, B. Bohn, S. Broch, H. Dong, G. I. Gkatzelis, T. Hohaus, F. Holland, X. Li, Y. Liu, Y. Liu, X. Ma, A. Novelli, P. Schlag, M. Shao, Y. Wu, Z. Wu, L. Zeng, M. Hu, A. Kiendler-Scharr, A. Wahner and Y. Zhang, Fast Photochemistry in Wintertime Haze: Consequences for Pollution Mitigation Strategies, *Environ. Sci. Technol.*, 2019, **53**, 10676–10684.

82 X. Peng, W. Wang, M. Xia, H. Chen, A. R. Ravishankara, Q. Li, A. Saiz-Lopez, P. Liu, F. Zhang, C. Zhang, L. Xue, X. Wang, C. George, J. Wang, Y. Mu, J. Chen and T. Wang, An unexpected large continental source of reactive bromine and chlorine with significant impact on wintertime air quality, *Natl. Sci. Rev.*, 2021, **8**, nwaa304.

83 G. He, J. Ma, B. Chu, R. Hu, H. Li, M. Gao, Y. Liu, Y. Wang, Q. Ma, P. Xie, G. Zhang, X. C. Zeng, J. S. Francisco and H. He, Inside Cover: Generation and Release of OH Radicals from the Reaction of H2O with O2 over Soot (Angew. Chem. Int. Ed. 21/2022), *Angew. Chem., Int. Ed.*, 2022, **61**, e202204829.

84 P. M. Edwards, S. S. Brown, J. M. Roberts, R. Ahmadov, R. M. Banta, J. A. deGouw, W. P. Dubé, R. A. Field, J. H. Flynn, J. B. Gilman, M. Graus, D. Helmig, A. Koss, A. O. Langford, B. L. Lefer, B. M. Lerner, R. Li, S.-M. Li, S. A. McKeen, S. M. Murphy, D. D. Parrish, C. J. Senff, J. Soltis, J. Stutz, C. Sweeney, C. R. Thompson, M. K. Trainer, C. Tsai, P. R. Veres, R. A. Washenfelder,

 

C. Warneke, R. J. Wild, C. J. Young, B. Yuan and R. Zamora, High winter ozone pollution from carbonyl photolysis in an oil and gas basin, *Nature*, 2014, **514**, 351–354.

85 K. Li, D. J. Jacob, H. Liao, Y. Qiu, L. Shen, S. Zhai, K. H. Bates, M. P. Sulprizio, S. Song, X. Lu, Q. Zhang, B. Zheng, Y. Zhang, J. Zhang, H. C. Lee and S. K. Kuk, Ozone pollution in the North China Plain spreading into the late-winter haze season, *Proc. Natl. Acad. Sci. U. S. A.*, 2021, **118**, e2015797118.

86 T. Wang, L. Xue, Z. Feng, J. Dai, Y. Zhang and Y. Tan, Ground-level ozone pollution in China: a synthesis of recent findings on influencing factors and impacts, *Environ. Res. Lett.*, 2022, **17**, 063003.